



**LABORATORY  
INVESTIGATION**  
THE SCIENCE THAT ADVANCES PATHOLOGY

# ABSTRACTS

(411-443)

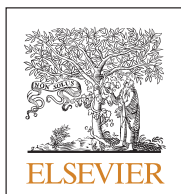
DERMATOPATHOLOGY



USCAP 113TH ANNUAL MEETING  
**BRINGING EDUCATION TO LIFE**

A stylized silhouette of a human head in profile, facing right. The interior of the head is filled with a dense forest of small trees, with a larger, more prominent tree growing from the top right. The background behind the head silhouette is a light beige color.

MARCH 23-28, 2024 | BALTIMORE, MD



 **USCAP** UNITED STATES AND CANADIAN  
ACADEMY OF PATHOLOGY

## EDUCATION COMMITTEE

**Rhonda K. Yantiss**  
Chair

**Carlos Parra-Herran**  
Chair, Abstract Review Board and Assignment Committee

**Laura C. Collins**  
Interactive Microscopy

**Carla L. Ellis**  
Chair, DEI Subcommittee

**Yuri Fedoriw**  
Short Course Coordinator

**Kristin C. Jensen**  
Chair, CME Subcommittee

**Ilan Weinreb**  
Chair, Subcommittee for Unique Live Course Offerings

**Adebowale J. Adeniran**

**Kimberly H. Allison**

**Phyu P. Aung**

**Justin A. Bishop**

**Marilyn M. Bui**

**Sarah E. Gibson**

**Jennifer B. Gordetsky**

**Melinda F. Lerwill**

**Chieh-Yu Lin**

**M. Beatriz S. Lopes**

**Tamara L. Lotan**

**Terri L. Mason**, Pathologist-in-Training

**Nicole C. Panarelli**

**Charles "Matt" Quick**

**David F. Schaeffer**

**Maria Westerhoff**

**Josh Alexander Zeitlin**, Pathologist-in-Training

## ABSTRACT REVIEW BOARD

Benjamin Adam  
Oyedele Adeyi  
Kenneth D. Aldape  
Mariam Priya Alexander  
F Zahra Aly  
Catalina Amador  
Vijayalakshmi Ananthanarayanan

Barina Aqil  
Manju Aron  
Ibrahim Batal  
Gregory R. Bean  
Govind Bhagat  
Amarpreet Bhalla  
Michael Bonert  
Tamar C. Brandler  
Allen P. Burke  
Kelly J. Butnor  
Sarah M. Calkins  
Weibiao Cao  
Barbara Ann Centeno  
Joanna SY Chan  
Vishal S. Chandan

Guoli Chen  
Hao Chen  
Lin Cheng  
Soo-Jin Cho  
Shefali Chopra  
John Chrsinger  
Adela Cimic  
Cecilia G. Clement  
Jennifer A. Cotter  
Luis E. De Las Casas  
Elizabeth G. Demicco  
Katie Dennis  
Jasreman Dhillon  
Anand S. Dighe  
Bojana Djordjevic  
Michelle R. Downes  
Siraj M. El Jamal  
Kim Adams Ely  
Mark G. Etel  
Sara M. Falzarano  
Fang Fan

Evan A. Farkash  
Gelareh Farshid  
Michael Feely  
Samson W. Fine  
Susan A. Fineberg  
Danielle Fortuna  
Monica T. Garcia-Buitrago  
Zeina Ghorab  
Alessio Giubellino  
Carolyn Glass  
Hamza N. Gokozan  
Carmen Gomez-Fernandez  
Shunyou Gong  
Purva Gopal  
Anne Grabenstetter  
Ian S. Hagemann  
Richard D. Hammer  
Suntrea TG Hammer  
Eyas M. Hattab  
Juan C. Hernandez-Prera  
Jonas J. Heymann  
Carlo Vincent Hojilla  
Jody E. Hooper  
Tao Huang  
Weei-Yuarn Huang  
Wei Huang  
Aaron R. Huber  
Kenneth A. Iczkowski  
Jabed Iqbal  
Shabnam Jaffer  
Shilpa Jain  
Jose Jessurun  
Ivy John  
Ridas Juskevicius  
Meghan E. Kapp  
Seema Kaushal  
Mahmoud A. Khalifa  
Thaer Khoury  
Benjamin Kipp  
Christian A. Kunder  
Stefano La Rosa  
Brandon T. Larsen  
Katsiaryna Laziuk

Goo Lee  
Vasiliki Leventaki  
Xiaoxian Li  
Mikhail Lisovsky  
Lesley C. Lomo  
Abberly Lott Limbach  
Scott B. Lovitch  
Fang-I Lu  
Changqing Ma  
Degin Ma  
Cristina Magi-Galluzzi  
Varsha Manucha  
Rachel Angelica Mariani  
L. Jeffrey Medeiros  
Anne M. Mills  
Kamran M. Mirza  
Hiroshi Miyamoto  
Kathleen T. Montone  
Kristen E. Muller  
Priya Nagarajan  
Asghar H. Naqvi  
Navneet Narula  
Dianna L. Ng  
Michiya Nishino  
Maura O'Neil  
Sanjay S. Patel  
Burcin Pehlivanoglu  
Deniz Peker Barclift  
Raghavendra Pillappa  
Andre Pinto  
Susan Prendeville  
Carlos N. Prieto Granada  
Bibianna M. Purgina  
Martha M. Quezado  
Emilian V. Racila  
Santiago Ramon Y Cajal  
Rema A. Rao  
Kaaren K. Reichard  
Jordan P. Reynolds  
Heesun J. Rogers  
Lisa Rooper  
Andrew Eric Rosenberg  
Esther Diana Rossi

Evita T. Sadimin  
Ozlen Saglam  
Ankur R. Sangoi  
Kurt B. Schaberg  
Vicki J. Schnadig  
Qiuying (Judy) Shi  
Wonwoo Shon  
Pratibha S. Shukla  
Gabriel Sica  
Anthony Sisk  
Kalliopi P. Siziopikou  
Stephanie Lynn Skala  
Isaac H. Solomon  
Wei Song  
T. Rinda Soong  
Simona Stolnicu  
Paul E. Swanson  
Ben Jack Swanson  
Sara Szabo  
Elizabeth D. Thompson  
Gulisa Turashvili  
Neha Varshney  
Jaylou M. Velez Torres  
Hanlin L. Wang  
He Wang  
Stephen C. Ward  
Kevin M. Waters  
Jaclyn C. Watkins  
Shi Wei  
Kwun Wah Wen  
Deyin Xing  
Bin Xu  
Ya Xu  
Shaofeng Yan  
Zhaohai Yang  
Feng Yin  
Ji (Jane) Yuan  
Huina Zhang  
Xuchen Zhang  
Bihong Zhao

To cite abstracts in this publication, please use the following format: Author A, Author B, Author C, Author D, et al.

Abstract title. *Laboratory Investigation*. 2024;104 (suppl 1):page#. File Title abstract #.

## 411 Clinicopathologic and Molecular Characterization of a Series of Sporadic Trichoblastic Neoplasms

Asma Abu-Salah<sup>1</sup>, Carina Dehner<sup>1</sup>, Brandon Umphress<sup>2</sup>, Ahmed Alomari<sup>1</sup>, Simon Warren<sup>1</sup>, Numrah Fadra<sup>3</sup>, Rohini Mopuri<sup>3</sup>, Ruifeng (Ray) Guo<sup>4</sup>

<sup>1</sup>Indiana University School of Medicine, Indianapolis, IN, <sup>2</sup>Indiana University, Indianapolis, IN, <sup>3</sup>Mayo Clinic, Rochester, MN, <sup>4</sup>Mayo Clinic, Jacksonville, FL

**Disclosures:** Asma Abu-Salah: None; Carina Dehner: None; Brandon Umphress: None; Ahmed Alomari: None; Simon Warren: None; Numrah Fadra: None; Rohini Mopuri: None; Ruifeng (Ray) Guo: None

**Background:** Trichoblastoma is a benign primitive follicular neoplasm that arises in the setting of Brooke-Spiegler syndrome (driven by pathogenic *CYLD* mutations), in association with nevus sebaceous (driven by mosaic *RAS* mutations), or sporadically, with so far poorly understood pathogenesis. We studied the histopathologic and molecular genetic features of 15 sporadic trichoblastic neoplasms including a rare case of trichogermanoma and a case of trichoblastic carcinoma arising within trichoblastoma.

**Design:** Institutional archives at two institutions were searched for “trichoblastoma/trichoblastic”. Tumors in the setting of Brooke-Spiegler syndrome or arising within nevus sebaceous were excluded. Available slides and blocks were retrieved. Clinical data was extracted from the electronic medical record systems. RNA sequencing (RNAseq) was performed on selected cases to assess for fusions, tumor mutational burden (TMB), and mutation signature (COSMIC).

**Results:** Fifteen tumors occurred in 9 males and 7 females with a median age of 64 years (range: 33-97) and involved the scalp (4), nasolabial fold (1), cheek (1), parotid (1), nasal ala (1), ear (1), upper chest (1), back (1), gluteal region (1), thigh (1), leg (1) and ankle (1). The median size was 1.6 cm (range: 1.2-7.0 cm). Clinical follow-up (15 patients; 100%; median: 65 months; range: 3-107 months) showed no evidence of disease at last follow-up. On histology, 13 tumors showed classic features of trichoblastoma, such as multinodular growth pattern, dermal location without epidermal connection, and surrounding fibrotic stroma. One case showed foci of increased atypia and mitotic activity, representing malignant transformation. One case demonstrated focal areas suggestive of “cell balls”, previously described in a rare variant of trichoblastoma, so-called trichogermanoma. RNAseq (6 tumors) revealed highly variable TMB and mutation signature related to DNA base excision repair and mismatch repair defect in all 6 cases (Fig. 1A, B). A recurrent *FOXK1::GRHL1* fusion was found in the case of trichogermanoma (2).

Figure 1 - 411

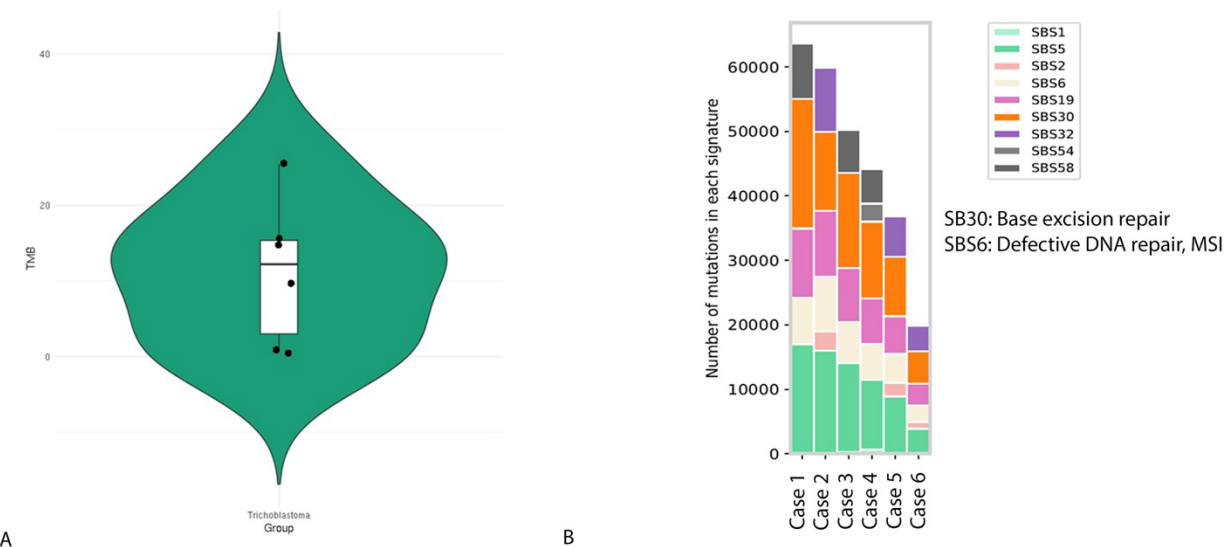
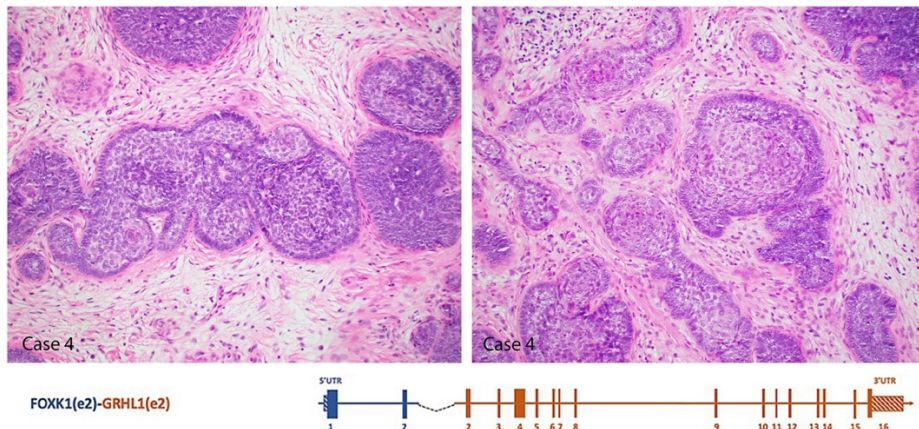


Figure 2 - 411



**Conclusions:** Herein, we report the histopathologic features of 15 cases of sporadic trichoblastic neoplasms. Among cases with gene expression profile, all tumors demonstrated consistent mutation signature associated with DNA repair defect and a case of trichogermanoma with *FOXK1::GRHL1* fusion. These findings shed light on molecular tumorigenesis which could potentially be of use for diagnostic practice. Larger scale validation studies are needed.

#### 412 Follicular Mucinosis and Cutaneous T-Cell Lymphoma Association: A Clinicopathologic and Molecular Analysis of 19 Cases

Ahmad Alshomrani<sup>1</sup>, Ketav Desai<sup>2</sup>, Allison Vokoun<sup>2</sup>, Ab Rauf Shah<sup>1</sup>, Ann Crowley<sup>3</sup>, Dinesh Pradhan<sup>1</sup>, Joseph Khoury<sup>1</sup>, Safina Hafeez<sup>4</sup>

<sup>1</sup>University of Nebraska Medical Center, Omaha, NE, <sup>2</sup>Nebraska Medical Center, Omaha, NE, <sup>3</sup>Nebraska Medicine, Omaha, NE <sup>4</sup>University of Nebraska Medical Center, Lincoln, NE

**Disclosures:** Ahmad Alshomrani: None; Ketav Desai: None; Allison Vokoun: None; Ab Rauf Shah: None; Ann Crowley: None; Dinesh Pradhan: None; Joseph Khoury: None; Safina Hafeez: None

**Background:** Follicular mucinosis is a rare dermatologic disorder characterized by the accumulation of mucin within hair follicles, resulting in distinct skin lesions. It can be associated with cutaneous T-cell lymphoma (CTCL), further complicating its clinical management and prognosis.

**Design:** We identified 19 cases of follicular mucinosis from 2010 to 2023. Hematoxylin and eosin (H&E) stained slides were reviewed to evaluate morphological features, including the presence of mucin within hair follicles and the extent of lymphocytic infiltrate. Immunostains for colloidal iron, Alcian blue, CD2, CD3, CD4, CD5, CD7, CD8, CD20, Granzyme, and TIA were performed in a subset of cases. T-cell receptor (TCR) gene rearrangement analysis was performed to investigate clonality.

**Results:** Patients aged 12 to 87 years (median age: 38), with 11 males (57.9%) and 8 females (42.1%), were included. Biopsies were obtained from various anatomical sites, with the back being the most sampled site (Table 1). All cases (100%) exhibited mucin accumulation within hair follicles, confirming follicular mucinosis by H&E staining. Immunostains were evaluated to rule out lymphoma, with additional staining (colloidal iron and Alcain blue) supporting mucin deposition. Two cases (10.5%) were associated with mycosis fungoides, and four cases (21.1%) were associated with atypical lymphoid proliferation. In the majority of cases (16/19, 84.2%), epidermotropism was not present. However, prominent epidermotropism occurred in 1/2 cases (50%) of mycosis fungoides and 1/4 cases (25%) of atypical lymphoid proliferation. Additionally, minimal epidermotropism was noted in one case (5.3%) of atypical lymphoid proliferation. TCR gene rearrangement analysis in 17 cases (89.5%) showed clonality in 9 cases (52.9%).

# ABSTRACTS | DERMATOPATHOLOGY

Table 1: Summary of the clinical and molecular features of follicular mucinosis and cutaneous T-cell lymphoma association

Cases	Age	Gender	Diagnosis	Anatomic Site	Epidermotropism	TCR Gene Rearrangement
1	17	M	follicular mucinosis	Forehead, thigh	Not present	Positive
2	35	F	follicular mucinosis with mycosis fungoides.	Back	Not present	Positive
3	66	M	follicular mucinosis	Back	Not present	Positive
4	47	M	follicular mucinosis	Temple	Not present	Negative
5	38	M	follicular mucinosis	Back	Not present	The quantity of T-cell-derived DNA was insufficient for a T-cell gene rearrangement study
6	38	M	follicular mucinosis	Back	Not present	Indeterminate for a clonal T-cell population
7	13	F	follicular mucinosis	Back	Not present	Negative
8	68	M	follicular mucinosis	Elbow	Not present	Negative
9	61	M	follicular mucinosis	Cheek	Not present	Suspicious but not diagnostic (small clonal population)
10	12	F	follicular mucinosis	Eyebrow	Not present	Not performed
11	13	M	follicular mucinosis	Cheek	Not present	Not performed
12	54	M	atypical lymphoid proliferation with follicular mucinosis	Scalp	Present	Positive
13	36	F	follicular mucinosis and atypical T-cell proliferation	Cheek	Not present	Positive
14	83	M	follicular mucinosis with mycosis fungoides	Back	Present	Positive
15	87	F	follicular mucinosis	Cheek	Not present	Positive
16	15	F	follicular mucinosis	Chin	Not present	Suspicious but not diagnostic (two sub-threshold peak)
17	49	F	follicular mucinosis	Labia Majora	Not present	negative
18	21	M	follicular mucinosis and atypical T-cell proliferation	Neck	Minimal epidermotropism	Positive
19	56	F	follicular mucinosis and atypical T-cell proliferation	Leg	Not present	Positive

**Conclusions:** The abstract offers a detailed clinicopathologic and molecular analysis of 19 cases of follicular mucinosis, with a particular focus on its association with CTCL, the utilization of immunohistochemistry, and molecular analysis. In cases of atypical lymphoid proliferation, TCR gene rearrangement analysis was positive. However, there was insufficient morphological evidence to make a diagnosis of lymphoma in the current biopsies. Therefore, close follow-up was recommended. Some follicular mucinosis cases may exhibit clonal TCR gene rearrangements without T-cell lymphoma evidence—referred to as pseudo-clonality or benign clonality. Distinguishing between true clonality and pseudo-clonality can be challenging.

**413 Superficial ALK-Rearranged Myxoid Spindle Cell Neoplasm: A Series of 32 Cases Highlighting a Morphologic and Molecular Genetic Spectrum with Epithelioid Fibrous Histiocytoma**Mia DeSimone<sup>1</sup>, Igor Odintsov<sup>1</sup>, Harrison Tsai<sup>1</sup>, Brendan Dickson<sup>2</sup>, Jason Hornick<sup>3</sup>, Christopher Fletcher<sup>1</sup>, David Papke<sup>1</sup><sup>1</sup>Brigham and Women's Hospital, Boston, MA, <sup>2</sup>Mount Sinai Health System, Toronto, Ontario, <sup>3</sup>Brigham and Women's Hospital, Harvard Medical School, Boston, MA**Disclosures:** Mia DeSimone: None; Igor Odintsov: None; Harrison Tsai: None; Brendan Dickson: None; Jason Hornick: None; Christopher Fletcher: None; David Papke: None**Background:** ALK rearrangements occur in an emerging family of kinase fusion-positive mesenchymal neoplasms, including epithelioid fibrous histiocytoma (FH) and the recently described superficial ALK-rearranged myxoid spindle cell neoplasm (ALKSCN). Here we expand upon the histopathologic, immunophenotypic, and molecular spectrum of ALKSCN.**Design:** Retrospective searches identified 32 cases from consultation and departmental archives. Patient demographics, tumor characteristics, and clinical outcome were ascertained when obtainable. Seventeen tumors were successfully sequenced using next-generation sequencing platforms (12 DNAseq, 5 RNAseq).**Results:** The cohort consisted of 17 females (53%) and 15 males, with a median age at presentation of 40 years (range: 6–82 yr). Most tumors occurred on the lower extremity (23 tumors; 72%), followed by upper extremity (4; 13%), trunk (3; 9%), and face (2; 6%). Tumors occurred primarily in the dermis (28 tumors; 88%) or subcutis (4; 13%); ten dermal tumors extended into the subcutis. Median tumor size was 1.2 cm (range: 0.5–7.0 cm). Histologically, tumors were characterized by bland spindle to ovoid cells showing whorled growth and myxoid to collagenous stroma. Recurrent features included perivascular hyalinization (19 tumors; 59%), epidermal collarette (16; 50%), amianthoid collagen (12; 38%), and bone formation (2; 6%). Immunohistochemistry (IHC) demonstrated expression of ALK (23/28), EMA (16/26), CD34 (14/19), and S-100 (11/31). Eleven tumors showed hybrid features between epithelioid FH and ALKSCN; most of these showed cytomorphology typical of epithelioid FH, but with whorled growth, myxoid stroma, and/or spindle cell features. Two hybrid tumors showed sharp transitions from a region of epithelioid FH to a region of ALKSCN, with a concomitant sharp transition in EMA, CD34, and S-100 expression. Sequencing revealed ALK fusions in 15/17 tumors: two each with fusion partners *FLNA*, *SQSTM1*, and *VCL*, and one each with *COL1A2*, *DCTN1*, *EML4*, *FXR1*, *MPRIP*, *PLEKHH2*, *PRKAR1A*, *SPECC1L*, and *TLN2*. Thirteen of 14 ALK-rearranged tumors expressed ALK by IHC. Two tumors negative for ALK fusions instead harbored *RET* fusions (*NCOA4::RET* and *TRIM27::RET*). *RET*-rearranged tumors were negative for ALK IHC. *CDKN2A/B* deletions were found in two tumors with ALK fusions and both tumors with *RET* fusions.**Conclusions:** ALKSCN is on a morphologic and molecular genetic spectrum with epithelioid FH, and some morphologically typical examples harbor alternate *RET* fusions.**414 Clinicopathologic and Molecular Characterization of Sun-Protected Basal Cell Carcinoma**Elizabeth Draper<sup>1</sup>, Yvonne Li<sup>2</sup>, Alvaro Laga<sup>3</sup>, John Hanna<sup>3</sup>, Eleanor Russell-Goldman<sup>3</sup><sup>1</sup>Brigham and Women's Hospital, Boston, MA, <sup>2</sup>Dana-Farber Cancer Institute, Boston, MA, <sup>3</sup>Brigham and Women's Hospital, Harvard Medical School, Boston, MA**Disclosures:** Elizabeth Draper: None; Yvonne Li: None; Alvaro Laga: None; John Hanna: None; Eleanor Russell-Goldman: None**Background:** Basal cell carcinoma (BCC), the most common skin cancer, is driven by UV-mediated Sonic Hedgehog (Hh) pathway mutations, most often involving PTCH1. Rarely, BCC can occur at sun-protected sites (i.e. genital and perianal BCC). This raises consideration of an alternative mechanism of pathogenesis in sun-protected BCC (SP-BCC). Here we use a next generation DNA sequencing (NGS) platform to compare the molecular pathogenesis of SP-BCC to conventional BCC, and we also describe the clinicopathologic features of SP-BCC.**Design:** We retrospectively identified 14 candidate SP-BCC cases. NGS was performed using a platform including the complete exonic DNA sequences of 447 cancer-related genes and 191 intronic regions across 60 genes to detect structural rearrangements and copy number variations. We also identified 8 conventional BCC with existing NGS data for comparison. Of note, Hh pathway genes including PTCH1, SUFU and SMO are included in this platform. In addition, we detail the clinicopathologic features of SP-BCC.**Results:** The clinicopathologic and genomic findings of SP-BCC are summarized in Table 1. A single patient (case 1) had a remote history of cobalt radiation to the anal area with subsequent development of a SP-BCC. For conventional BCC, tumor sites included metastatic site (n=3), trunk (n=3), and head/neck (n=2). None of the SP-BCC harbored a UV mutation signature, in contrast to all

# ABSTRACTS | DERMATOPATHOLOGY

conventional BCC cases. Thirteen SP-BCC cases had PTCH1 genomic alterations (13/14, 93%), and a subset harbored recurrent PTPN14 genomic alterations (4/14, 29%). All conventional BCC cases had PTCH1 alterations (8/8, 100%), but none had PTPN14 alterations (0/8, 0%). Management of SP-BCC included Mohs surgery (4/14; 29%); surgical excision (8/14; 57%); surgical excision and sentinel node biopsy (1/14; 7%) and no treatment (1/14; 7%). Recurrence was seen in 4/14 (29%) of SP-BCC cases, with a median follow-up of 18 months (range: 6 months to 9 years).

Table 1. Clinicopathologic and Genomic Characteristics of Sun-Protected Basal Cell Carcinoma						
Case	Age (Y)/sex	Anatomic Site	Molecular Alterations	Significance	Management & Outcome	Follow-Up Interval
1	60/F	Perianal	PTCH1 c.1847+1G>C ()  PTPN14 c.551_559del (p.Q184_S186del)  PTPN14 c.324_325delinsAT (p.W108_L109delins*)  PTPN14 c.491_492del (p.E164Vfs*38)	Splice site variant likely leads to loss of function.  High allele fraction suggestive of copy-neutral loss of heterozygosity and biallelic inactivation of PTCH1.	Mohs, no recurrence.	6 years
2	68/M	Perianal	PTCH1 c.1999G>T (p.E667*)  Single copy deletion of PTCH1 at 9q22.32	In-frame deletion of unclear significance.  Two frameshift variants likely lead to loss of function and suggest biallelic inactivation of PTPN14.	Mohs, no recurrence.	5 years
3	61/F	Perianal	PTCH1 c.666T>A (p.Y222*)  Single copy deletion of PTCH1 at 9q22.32	Splice site variant likely leads to loss of function.  SNP frequencies on chr 9q suggest copy neutral loss of heterozygosity and biallelic inactivation of PTCH1.	Excision, no recurrence.	2 years
4	90/M	Perianal	PTCH1 c.1341dup (p.L448Tfs*49)  Single copy deletion of PTCH1 at 9q22.32	Single copy deletion of unclear significance.	Excision with recurrence.	3 years
5	43/F	Vulva	PTCH1 c.1634_1645del (p.G545_V548del)  NOTCH1 c.3283G>A (p.D1095N)	Nonsense variant likely leads to loss of function.	Simple vulvectomy, no recurrence.	1 year
6	69/F	Vulva	PTCH1 c.591G>A (p.W197*)  Single copy deletion of PTCH1 at 9q22.32	Frameshift variant likely leads to loss of function.  Concurrent loss of PTCH1 is suggestive of biallelic loss of function.	Excisional biopsy, subsequent wide excision with recurrence.	2 years
7	79/F	Vulva	PTCH1 c.2098C>T (p.Q700*)  Single copy deletion of PTCH1 at 9q22.32	In-frame indel variant, likely pathogenic.	Radical vulvectomy, no recurrence.	1 year
8	66/F	Vulva	PTCH1 c.2524G>T (p.E842*)  Single copy deletion of PTPN14 at 1q41	Missense variant of unclear significance.	Mohs, no recurrence.	2 years
9	76/M	Scrotum	PTCH1 C.883G>A (p.W278*)  Single copy deletion of PTCH1 at 9q22.32	Nonsense variant likely leads to loss of function.	Mohs, no recurrence.	6 months
10	80/M	Scrotum	PTCH1 c.1752_1760del (p.N584_M587delinsK)  PTPN14 c.669+1G>A ()  PTPN14 c.442G>A (p.A148T)	Nonsense variant and single copy deletion suggestive of biallelic inactivation of PTCH1.	Excision, no recurrence.	9 years
11	62/M	Scrotum	PTCH1 c.1752_1760del (p.N584_M587delinsK)  Single copy deletion of PTCH1 at 9q22.32	Nonsense variant likely leads to loss of function.	None	6 months
12	80/F	Perianal	PTCH1 c.2524G>T (p.E842*)  Single copy deletion of PTCH1 at 9q22.32	Missense variant of unknown significance and deletion of PTCH1, may lead to loss of function.	Excision, no recurrence.	1 year
13	80/M	Perianal	PTCH1 c.1752_1760del (p.N584_M587delinsK)  PTPN14 c.669+1G>A ()  PTPN14 c.442G>A (p.A148T)	in-frame indel variant and likely copy-neutral loss of heterozygosity at this locus, likely biallelic alteration of PTCH1.  Splice site variant likely leads to loss of function.  Missense variant of unknown significance.	Excision with recurrence.	1 year
14	27/F	Perianal	PTCH1 c.2028C>A (p.Y676*)  PTPN14 c.1456_1477 del (p.S486gFS*45)	Nonsense variant likely leads to loss of function and loss of heterozygosity of chromosome 9q, likely biallelic inactivation of PTCH1  Frameshift variant likely leads to loss of function.	Excision and sentinel node biopsy, no recurrence.	1 year

Abbreviations: SNP, single nucleotide polymorphism.

**Conclusions:** We describe recurrent Hh pathway alterations in SP-BCC, namely in the PTCH1 gene, supporting their classification in the BCC family. All SP-BCC lacked evidence of a UV mutation signature, suggesting an alternative mechanism of mutagenesis in these tumors. SP-BCC appeared to be enriched for PTPN14 alterations, although PTPN14 alterations are described in the literature in BCC. SP-BCC can be locally aggressive tumors. Notably, the presence of PTCH1 mutations in SP-BCC confirms their susceptibility to Hh pathway inhibitors such as vismodegib.

#### 415 Quantification of Tumor Infiltrating lymphocytes (TILs) in Melanoma Using Artificial Intelligence: Potential for New Grading Schemes to Predict Outcome

Rofyda Elhalaby<sup>1</sup>, Priyadarshini Sivasubramaniam<sup>2</sup>, Roland Tian<sup>1</sup>, Václav Stejskal<sup>3</sup>, Christopher Hartley<sup>1</sup>

<sup>1</sup>Mayo Clinic, Rochester, MN, <sup>2</sup>Froedtert and the Medical College of Wisconsin, Milwaukee, WI, <sup>3</sup>University Hospital Hradec Králové, Hradec Králové, Czech Republic

**Disclosures:** Rofyda Elhalaby: None; Priyadarshini Sivasubramaniam: None; Roland Tian: None; Václav Stejskal: None; Christopher Hartley: None

**Background:** Melanoma was one of the earliest tumors considered for immune checkpoint inhibitor (ICI) therapy given its highly immunogenic nature. The presence of an inflamed tumor microenvironment correlates with response to therapy. Previously proposed grading methods for TILs were semi-quantitative and somewhat subjective. Our aim was to utilize artificial intelligence (AI) in developing a deep learning-based model to identify and quantify TILs in melanoma.

**Design:** Whole slide images (WSI) in the TCGA melanoma databased were reviewed, and 57 cases of primary tumor with optimal tissue quality were selected. Digitized images were then uploaded to Aiforia cloud-based image analysis platform (Aiforia Inc., Cambridge, MA, USA). The training set included 20 representative images and a layer tree was assembled in a hierarchical fashion (Figure 1) to train convolutional neural networks (CNNs) to recognize 9 region or object feature layers. Hand-drawn annotations constituted the learning input and training was done in 6 consecutive cycles with gradually increasing iterations and additional annotations based on feedback from the verification and analysis results. Training region covered 863.55 mm<sup>2</sup> and 5650 objects (5220 tumor cells and TILs and 430 stromal infiltrating lymphocytes/SILs). Finally, adequate performance was achieved, and image analysis was run on the entire dataset.

**Results:** Model performance metrics in training regions was generated for each layer/class using the verification tool. The overall accuracy (F1 score) for both tumor cells and lymphocytes was 98.63%, with total error of 2.7% (141/5220). F1 score for the tumor, stroma and lymphoid aggregate sublayer was 95.95% (total error 5.78%, 2.13/36.84 mm<sup>2</sup>) (table 1). The mean TIL counts/tumor area was 391.85 (17.93-1475.38 range and SD ± 345.00) while the mean tumor cell count/tumor area was 3809.57 (770.32-6242.02 range and SD ± 1071.87). None of the normalized tumor cell counts or TILs counts were significantly correlated with survival or tumor mutational burden (data not shown).

Verification metrics for assessment of model performance in training regions							
Features/ layer	False Positive (%)	False Negative (%)	Precision (%)	Sensitivity (%)	Specificity (%)	Total Error (%)	F1-score (%)
<b>Normal</b>	0.01	0.67	99.99	99.33	99.99	0.68	99.66
<b>Total Tumor</b>	0.05	0.94	99.95	99.06	99.95	0.99	99.50
<b>Tumor</b>	0.51	2.80	99.48	97.20	99.49	3.31	98.33
<b>Lymphoid aggregate</b>	24.37	28.69	74.53	71.31	75.63	53.06	72.89
<b>Stroma</b>	4.01	26.45	94.83	73.55	95.99	30.46	82.85
<b>Tumor cells</b>	0.05	2.66	99.95	97.34	99.95	2.70	98.63
<b>TILs</b>	0.11	2.59	99.88	97.41	99.89	2.70	98.63
<b>SILs</b>	0	35.81	100	64.19	100	35.81	78.19
Image analysis results (n=57)							
	Tumor area (mm <sup>2</sup> )		TILs		Tumor cells		
			Counts	Percentage	Counts	Percentage	
<b>Range</b>	10.95-158.83		17.93-1475.38	0.55-32.72	770.32-6242.02	67.28-99.45	
<b>Mean</b>	64.82		391.85	8.89	3809.57	91.11	
<b>Median</b>	62.26		288.61	7.07	3828.11	92.93	
<b>SD</b>	34.19		345.00	6.59	1071.87	6.59	

Figure 1 - 415

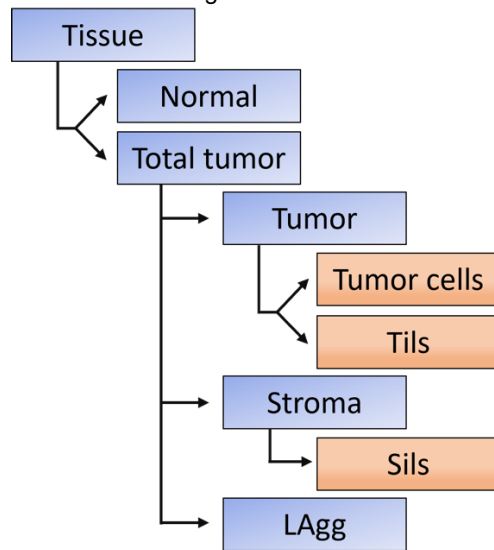


Figure (1): Algorithm layer tree demonstrating a hierarchy of parent layers/classes and child sublayers, blue boxes represent the “regions” layers and orange boxes indicate the “object counter/detector” layers.  
 (TILs): Tumor infiltrating lymphocytes, (SILs): Stromal infiltrating lymphocytes  
 and Lagg (Lymphoid aggregates)

Figure 2 - 415

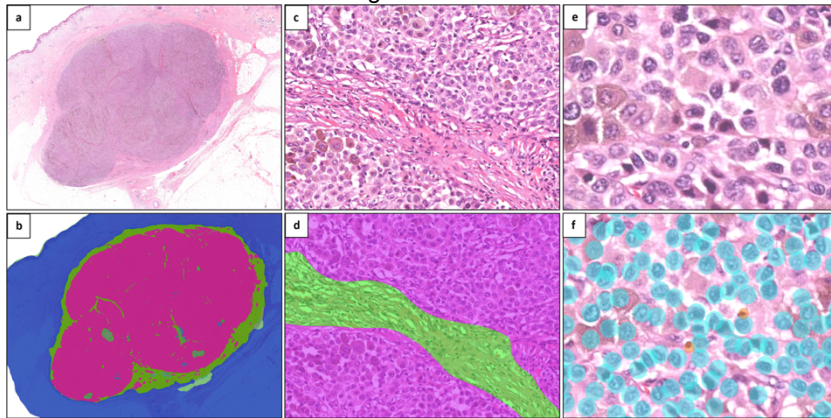


Figure (2): Snapshots from Aliforia's platform showing H&E-stained slide (a), tumor is a fairly defined mass in the deep dermis and upper subcutis. Heat map for all the feature layers (image b) showing distinction between Normal (blue), Tumor (purple) and Stoma (green). Images (c) and (d) show the same focus before and after applying the heat map, with the tumor with demarcated tumor and stromal compartments. Closer view on tumor area (image e), the object detector shows mixed population of tumor cells (blue circles) and lymphocytes (orange circles).

**Conclusions:** TIL density in melanoma shows wide variability, which may form the basis for differences in response to ICI. Attempts at precise manual quantification are rather impractical, which makes AI models more time efficient quantification tools. Application of AI-powered models can help establish novel grading criteria. As our current metrics did not correlate with survival or TMB, we plan to apply a more sophisticated analysis of TILs and lymphoid aggregates.

#### 416 Evaluation of an Investigational Software for Analysis of Microsatellite Instability in Multiple Cutaneous Cancers

Robert Emerson<sup>1</sup>, Thomas Davis, Justin Lemke<sup>2</sup>, Eshwar Udho<sup>2</sup>

<sup>1</sup>Indiana University School of Medicine, Indianapolis, IN, <sup>2</sup>Promega Corporation, Madison, WI

**Disclosures:** Robert Emerson: None; Thomas Davis: None; Justin Lemke: None; Eshwar Udho: None

**Background:** Emerging evidence indicates that microsatellite instability (MSI) may be associated with Lynch Syndrome across cancer types, not just in colorectal carcinoma and endometrial carcinoma. Interest in detection of MSI in tumors other than

## ABSTRACTS | DERMATOPATHOLOGY

colorectal and endometrial carcinoma is increasing as immunotherapeutic approaches are being developed for MSI-high (MSI-H) tumors of diverse types. The goal of this research study is to validate a polymerase chain reaction (PCR)-based method of detecting microsatellite instability in cutaneous tumors through comparison with immunohistochemical (IHC) analysis of mismatch repair (MMR) proteins.

**Design:** We identified tumor specimens from adult patients including 17 Merkel cell carcinomas, 27 sebaceous carcinomas, 30 melanomas, and 29 vulvar squamous cell carcinomas. Specimens with an adequate tumor block (greater than 20% tumor) and a normal tissue block were included. Paraffin curls of tumor and normal tissue for each specimen were analyzed using the Applied Biosystems 3500 Dx Genetic Analyzer using the OncoMate® MSI Dx Analysis System and determined to be MSI-H or microsatellite stable (MSS) with an investigational data interpretation software currently under development at Promega. For tumors that had not been evaluated previously by MMR, sections of tumor were stained for MMR-associated proteins. If at least one MMR marker showed loss of expression, the case was considered to show MMR loss.

**Results:** Of the 103 samples, 88 (85%) could be evaluated for MSI by PCR and in 15 the results were considered invalid. Of these, 87 cases had sufficient material for MMR staining and 1 did not. The MSI results correlated with MMR IHC results in 82 cases (94%) and did not correlate in 5 cases (6%). There were 14 correlating MSI-H/MMR-loss cases, 68 correlating MSS/MMR-retained cases, and 5 non-correlating MSS/MMR-loss cases. There were no non-correlating MSI-H/MMR-retained cases. MSI-H was identified in 1 of 13 Merkel cell carcinomas (8%), 13 of 26 sebaceous carcinomas (50%), 0 of 23 melanomas, and 0 of 26 vulvar squamous cell carcinomas.

**Conclusions:** PCR analysis using the Promega OncoMate® MSI Dx Analysis System with an investigational data interpretation software correlates with evaluation of MMR expression by IHC in 94% of cases, among the tumor types evaluated. MSI-high results reliably (100% in this sample) predict loss of MMR protein IHC staining, but occasional cases yield MSS results while having MMR loss by IHC.

### 417 The Microenvironment in Transformed Mycosis Fungoides: Potential Prognostic Factors and Therapeutic Targets

Anna Sarah Erem<sup>1</sup>, Ishaq Asghar<sup>2</sup>, Pamela Allen<sup>2</sup>, Saja Asakrah<sup>3</sup>

<sup>1</sup>Emory University School of Medicine, Atlanta, GA, <sup>2</sup>Emory University, Atlanta, GA, <sup>3</sup>Emory University Hospital, Atlanta, GA

**Disclosures:** Anna Sarah Erem: None; Ishaq Asghar: None; Pamela Allen: None; Saja Asakrah: None

**Background:** Mycosis fungoides (MF) with large cell transformation leads to poor survival. Prognostic factors include CD30 negativity, stage IIb-IV, and folliculotropic variant. Despite advances in targeted immunotherapy, MF remains incurable, particularly in advanced stages. Research on tumor microenvironment (TME) reveals mechanisms behind immune dysregulation. This study delves into the MF's immune microenvironment to uncover disease pathogenesis and potential treatment avenues.

**Design:** We reviewed Epic patient charts diagnosed with mycosis fungoides. Factors like large cell percentage, CD30, and disease stage at biopsy were examined. RNA extracted from tissues underwent analysis with the nCounter pan-cancer immune profiling panel, processed by ROSALIND® with QC measures. Data was normalized using Nanostring criteria.

**Results:** 31 patients with MF were identified. Large cell transformation was seen in 14 patients. Two cases lacked staging information. 17 cases didn't show significant large cell transformation (large cells <5%-10%). 71% transformed MF cases had CD30 immunostaining ≥ 10%, and 57% were in advanced stages. In non-transformed cases, 18% had CD30 > 10% and 33% were in advanced stages. Genomic analysis revealed overexpression of NKG2 family genes (KLRC1, KLRC2, KLRK1) with significant p values. T-reg and Foxp3 genes were less expressed in transformed cases, while CD164 showed overexpression.

Patient No	Age at diagnosis	Stage at time of biopsy	Large cell % at time of biopsy	Large cell transformation	CD30 % at time of biopsy
1	65	4a1	30%	MF-T	30%
2	66	4b	50%	MF-T	2%
3	13	2a	30%	MF-T	1%
4	45	1a	40%	MF-T	40%
5	57	1a	30%	MF-T	40%
6	31		75%	MF-T	75%
7	48	2b	25%	MF-T	48%
8	37	1b	25%	MF-T	10%
9	58		35%	MF-T	75%
10	45	2b	30%	MF-T	5%
11	39	2b	30%	MF-T	5%
12	47	4a	40%	MF-T	75%
13	70	4a2	30%	MF-T	50%
14	49	2b	25%	MF-T	15%
15	57	4a2	5%	MF	5%
16	53	2b	1%	MF	1%
17	51	1b	10%	MF	20%
18	21	2b	1%	MF	1%
19	35	2b	5%	MF	2%
20	40	1b	1%	MF	1%
21	40	3a	5%	MF	40%
22	38	3a	5%	MF	20%
23	59		1%	MF	5%
24	73	1a	1%	MF	1%
25	57	2a	1%	MF	1%
26	66	3a	1%	MF	5%
27	31	1a	1%	MF	1%
28	48	2a	1%	MF	2%
29	81	2a	1%	MF	1%
30	62	2a	1%	MF	1%
31	74	1b	1%	MF	5%

Figure 1 – 417

**Figure 1 Differential expression data between transformed MF and non-transfomed MF**

Name	Description	Fold-change	p-value
KLRC1	Killer cell lectin-like receptor subfamily C, member 1	4.0982	0.00456
KLRC2	Killer cell lectin-like receptor subfamily C, member 2	6.13618	0.00516
KLRK1	Killer cell lectin-like receptor subfamily K, member 1	2.71449	0.02079

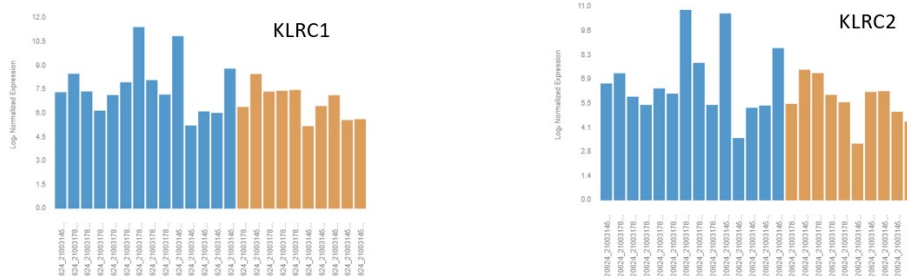


Figure 2 – 417

## Cell Type Profiling

The cell abundance scores for all samples in your experiment are displayed below and grouped by cell type. Cell Type Scores are based on the NanoString Cell Type Profiling Module. Two-color heatmaps show scores normalized across all samples. You may filter results by entering either one term name, or a list of terms separated by commas.

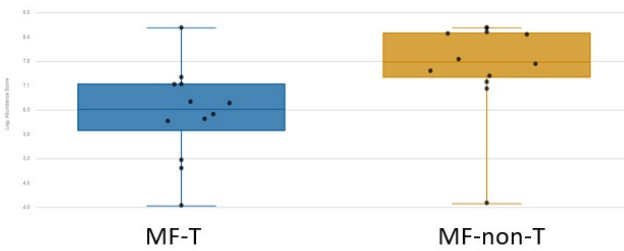


Fig-2A  
① Treg

## Gene Expression Data

The normalized expression levels for all samples in your Experiment are displayed below. You may search for gene(s) by entering either one gene symbol, or a list of gene symbols separated by commas.

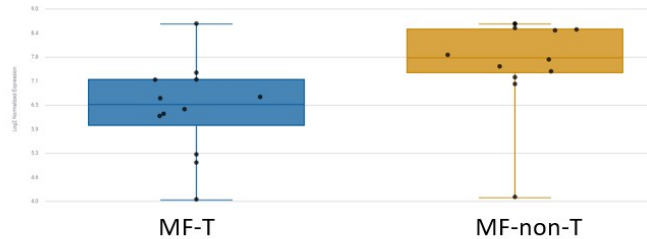


Fig-2B  
① FOXP3

**Conclusions:** NKG2A, found on natural killer cells and T-cells, inhibits NK cell activity. Monalizumab, an antibody targeting CD94/NKG2A, shows promise in solid tumors and lymphomas but is unexplored in MF. Our findings suggest potential benefits of Monalizumab in transformed MF. Fewer T-regulatory cells with Foxp3 expression in transformed MF indicates their role in suppressing neoplastic T-cell progression. CD164 impacts hematopoietic progenitor cell functions, and its high expression links to Sezary syndrome. This study noted raised CD164 expression in transformed cases, hinting at poor prognosis. However, our study's small sample size necessitates further large-scale research.

## 418 Utility of Immunohistochemistry in the Diagnosis of Porocarcinoma and Other Cutaneous Neoplasms

Anna Sarah Erem<sup>1</sup>, Di Ai<sup>2</sup>, George Birdsong<sup>3</sup>, Zachary Wolner<sup>1</sup>, Andrew Bellizzi<sup>4</sup>, Douglas Clark Parker<sup>5</sup>

<sup>1</sup>Emory University School of Medicine, Atlanta, GA, <sup>2</sup>McGovern Medical School at UTHealth, The University of Texas Health Science center at Houston, Houston, TX, <sup>3</sup>Emory University School of Medicine, Grady Memorial Hospital, Atlanta, GA, <sup>4</sup>University of Iowa Hospitals & Clinics, Iowa City, IA, <sup>5</sup>Emory University, Atlanta, GA

**Disclosures:** Anna Sarah Erem: None; Di Ai: None; George Birdsong: None; Zachary Wolner: None; Andrew Bellizzi: None; Douglas Clark Parker: None

**Background:** Eccrine porocarcinoma (EPC) is a rare, cutaneous adnexal neoplasm with a reported rate of 20-30% metastasis to lymph nodes. EPC may arise de novo or in association with a poroma. Differentiating EPC from other cutaneous epithelial neoplasms, including other malignant adnexal tumors, poorly differentiated squamous cell carcinoma (pdSCC), and metastatic carcinoma, can be challenging. Molecular advances have found YAP1::NUTM1 fusions are more common in EPCs and YAP1::MAML2 in poromas.

**Design:** Evaluate the utility of YAP1 C-terminus, YAP1 N-terminus and NUT immunohistochemistry (IHC) on tissue microarray samples of cutaneous neoplasms. A search of our pathology database identified 13 EPCs (9 arising in association with a poroma), 24 poromas, 15 pdSCCs, 7 hidradenocarcinomas, and 9 sebaceous carcinomas (SC). Furthermore, we evaluated the utility of IHC for c-KIT, CEA, EMA, p40 and PRAME in EPCs and other cutaneous neoplasms.

**Results:** Seven of 13 (54%) EPCs had a complete loss of YAP1-C expression, of which 6 (46%) demonstrated strong nuclear NUT positivity, confirming the YAP1::NUTM1 fusion. One case (8%) with loss of YAP1-C had no NUT expression, consistent with YAP1 fusion with a non-NUT partner. One (8%) EPC showed YAP1-C retention with NUT positivity, suggesting a NUT fusion with a different partner. All YAP1 fusion associated EPCs rose in association with a poroma. The majority of poromas (71%) had loss of YAP1 without NUT expression, consistent with YAP1 fusion with a different partner. Four of 24 (17%) poromas had loss of YAP1-C and NUT positivity. One of 13 EPC patients (8%) had local recurrence with lymph node metastasis, while 3 (23%) passed away. None of those patients had YAP1 or NUT fusion. All pdSCCs, hidradenocarcinomas and SCs were NUT negative with strong YAP1-C expression. YAP1 N-terminus was positive in all tumors. C-KIT was positive in 71% EPCs, while only 20% pdSCCs were focally positive. C-KIT was negative in all other tumors. PRAME was only positive in all SCs.

YAP-C Terminus NUT IHC patterns:		EPCs (n=13)	Poromas (n=24)	pdSCC (n=15)	HACs (n=7)	Sebaceous Carcinoma (n=9)
YAP-C <sup>lost</sup> /NUT <sup>pos</sup>	<i>YAP1::NUTM1</i>	6/13 (46%)	4/24 (17%)	0/15 (0%)	0/7 (0%)	0/9 (0%)
YAP-C <sup>lost</sup> /NUT <sup>neg</sup>	YAP with non-NUT partner	1/13 (8%)	17/24 (71%)	0/15 (0%)	0/7 (0%)	0/9 (0%)
YAP-C <sup>Retained</sup> /NUT <sup>pos</sup>	NUT with non-YAP partner	1/13 (8%)	0/24 (0%)	0/15 (0%)	0/7 (0%)	0/9 (0%)
YAP-C <sup>Retained</sup> /NUT <sup>neg</sup>	No Known Fusion	5/13 (38%)	3/24 (13%)	15/15 (100%)	7/7 (100%)	9/9 (100%)
<b>Additional IHCs:</b>						
YAP-N Terminus		13/13 (100%)	23/24 (96%)	15/15 (100%)	7/7 (100%)	9/9 (100%)
c-KIT		10/13 (77%)	17/24 (71%)	3/15 (20%)	4/7 (57%)	0/9 (0%)
p40		13/13 (100%)	24/24 (100%)	15/15 (100%)	7/7 (100%)	9/9 (100%)
EMA		13/13 (100%)	18/24 (75%)	12/15 (80%)	6/7 (86%)	9/9 (100%)
CEA		10/13 (77%)	17/24 (71%)	0/15 (0%)	3/7 (43%)	0/9 (0%)
PRAME		0/13 (0%)	0/24 (0%)	0/15 (0%)	0/7 (0%)	9/9 (100%)

**Conclusions:** The combination of YAP1 C-terminus and NUT IHC demonstrates diagnostic utility for tumors of poroid origin, including EPC. The presence of pre-existing poroma in all EPCs with *YAP1::NUTM1* fusion suggests increased risk of developing EPC from poromas with this fusion. Other YAP-associated fusions have a lower risk of transformation. In clinical follow up, EPCs lacking YAP or NUT fusions showed more aggressive behavior.

#### 419 Unique Genomic Alterations Characterize Undifferentiated Melanoma

Grant Fischer<sup>1</sup>, Navin Mahadevan<sup>2</sup>, Jason Hornick<sup>3</sup>, Christopher Fletcher<sup>1</sup>, Eleanor Russell-Goldman<sup>3</sup>

<sup>1</sup>Brigham and Women's Hospital, Boston, MA, <sup>2</sup>Dana-Farber Cancer Institute, Brigham and Women's Hospital, Harvard Medical School, Boston, MA, <sup>3</sup>Brigham and Women's Hospital, Harvard Medical School, Boston, MA

**Disclosures:** Grant Fischer: None; Navin Mahadevan: None; Jason Hornick: None; Christopher Fletcher: None; Eleanor Russell-Goldman: None

**Background:** Undifferentiated melanoma (UM) is defined as melanoma which has lost phenotypic and immunohistochemical features of conventional melanoma (CM). A subset of UM harbor *BRAF* or *NRAS* mutations, yet there is a paucity of data describing alterations unique to UM. We directly compare the molecular profiles of UM to CM to provide novel insights into UM-specific pathogenesis.

**Design:** This retrospective study included 10 UMs, selected based on exclusion of alternative diagnoses, the presence of melanoma-associated drivers and a history of melanoma in a subset of cases. Available sequencing data of 119 CMs was compared. Targeted sequencing of 447 cancer-associated genes was performed, including identification of mutations and somatic copy number alterations (CNAs). Variants classified as "Tiers 1-3" (Joint Consensus Guidelines) were included in downstream analyses along with "Tier 4" variants predicted to be pathogenic by the Cancer Genome Interpreter workspace. Statistical analyses were performed in R (v4.3.1) and SPSS (v29.0). The clinicopathologic features of the UM cohort are also described.

**Results:** The clinicopathologic features of the UM cohort are described in Table 1. Recurrent pathogenic variants and the most recurrent CNAs are shown in Fig. 1 & 2. *NRAS* was the most frequent driver in UM. Compared to CMs, UMs demonstrated nominally significant enrichment of pathogenic variants in *RAC1* (OR=19.1, p<0.001), *TP53* (OR=5.5, p<0.05), and *NRAS* (OR=3.931, p<0.05). *RAC1* remained statistically significant after multiple hypothesis testing correction on univariable analysis (FDR q-val<0.05) and after correcting for patient age and primary/metastatic status of samples in a multivariable model (OR=20.4, p<0.001). UMs also showed statistically significant (FDR q-val<0.05) enrichment of low-level gains in *WWTR1* and heterozygous deletions of *FOXO1*, *FIP1L1*, and *FAM175A*.

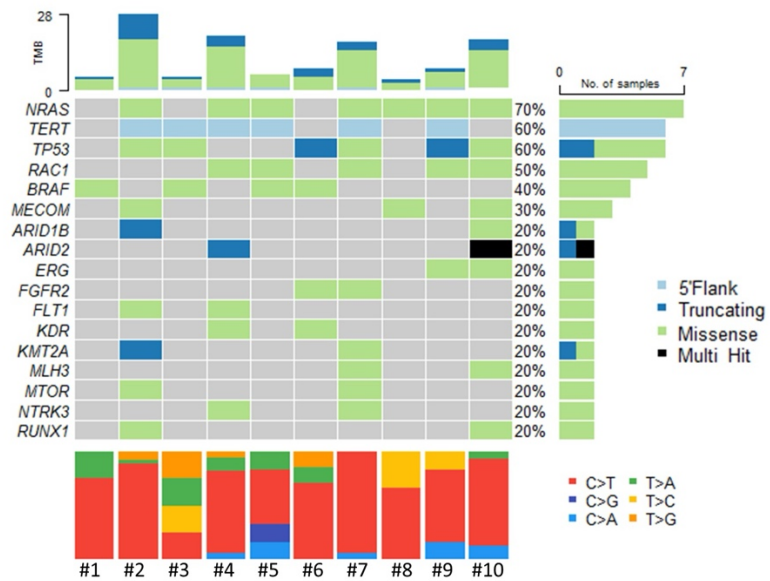
Table 1. Clinicopathologic Features of the Undifferentiated Melanoma Cohort

Case	Sex/Age (years)	Anatomic Site	Tumor Type	MAP Kinase Pathway Alteration	RAC1 Alteration	BRAF V600E IHC	NRAS Q61R IHC
1	M/61	Skin, back	Primary	BRAF c.1799T>A (p.V600E)	-	Positive	Not done
2	M/67	Skin, postauricular	Recurrence	NRAS c.37_38delinsTA (p.G13Y)	-	Negative	Negative
3	M/74	Neck LN	Metastasis	BRAF c.1798_1799delinsAA (p.V600K)	-	Negative	Negative
4	M/76	Skin, back	Recurrence	NRAS c.182A>T (p.Q61L)	RAC1 c.86C>T (p.P29L)*	Negative	Negative
5	M/40	Colon	Metastasis	BRAF c.1799T>A (p.V600E) NRAS c.37G>C (p.G13R)	RAC1 c.33C>A (p.D11E)*	Negative	Negative
6	M/57	Axillary soft tissue	Metastasis	BRAF c.1799T>A (p.V600E)	-	Negative	Negative
7	F/71	Pelvis	Metastasis	NRAS c.181C>A (p.Q61K)	RAC1 c.85C>T (p.P29S)*	Negative	Negative
8	F/76	Pelvis	Metastasis	NRAS c.38G>A (p.G13D)	-	Negative	Negative
9	F/60	Kidney	Metastasis	NRAS c.182A>G (p.Q61R)	RAC1 c.85C>T (p.P29S)*	Negative	Positive
10	M/82	Skin, scalp	Primary	NRAS c.182A>T (p.Q61L)	RAC1 c.85C>T (p.P29S)*	Negative	Negative

Abbreviations: MAP; mitogen activated kinase. IHC; immunohistochemistry. LN; lymph node.

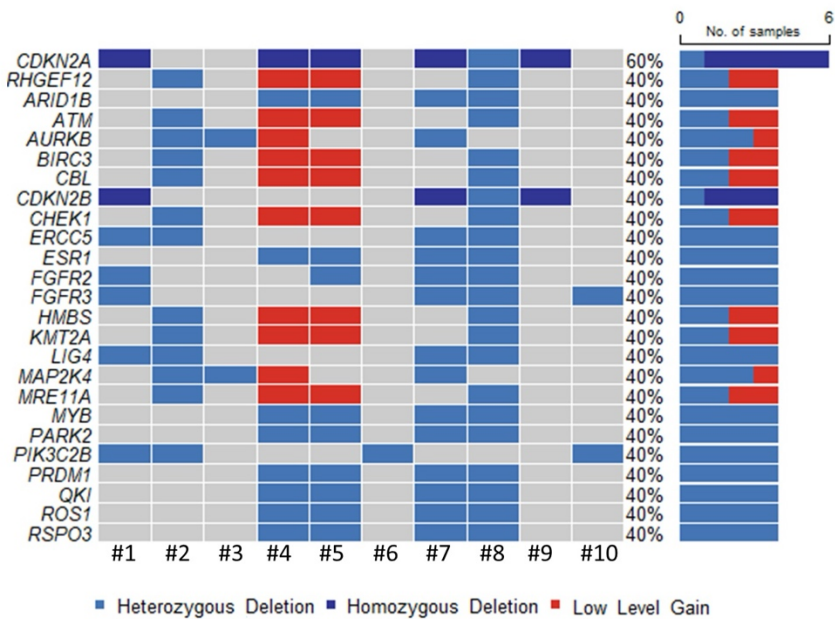
\*These RAC1 mutations have been previously described as pathogenic.

Figure 1 – 419



**Figure 1.** All genes with recurrent pathogenic nonsynonymous mutations from 10 UMs profiled via targeted exome sequencing. Truncating mutations include nonsense, frameshift, splice site, and splice region mutations.

Figure 2 - 419



**Figure 2.** Top 25 genes with copy number alterations from 10 UMs profiled via targeted exome sequencing. High level amplifications were not identified in these genes.

**Conclusions:** We show that UMs harbor distinct genomic aberrations including enrichment of non-Q61R *NRAS* mutations. This has important diagnostic implications as NRASQ61R immunohistochemistry, often critical for the diagnosis of UM, is negative in these cases. The presence of recurrent and potentially targetable *RAC1* mutations in UM is a notable finding with both diagnostic and therapeutic implications. Furthermore, *RAC1* P29S mutations have been shown to drive a melanocytic to mesenchymal switch in melanocytes, offering a possible explanation for the undifferentiated phenotype of these melanomas.

**420 CD140b (PDGF Receptor beta) is a Sensitive and Potentially Useful Marker for Atypical Fibroxanthoma/Pleomorphic Dermal Sarcoma**

Tayler Gant<sup>1</sup>, Wonwoo Shon<sup>1</sup>

<sup>1</sup>Cedars-Sinai Medical Center, Los Angeles, CA

**Disclosures:** Tayler Gant: None; Wonwoo Shon: None

**Background:** Atypical fibroxanthoma (AFX) and pleomorphic dermal sarcoma (PDS) are closely related tumors, believed to represent a continuum of the same neoplastic process, sharing numerous clinical features as well as morphological, immunohistochemical, and genetic characteristics. Because AFX/PDS often remains a diagnosis of exclusion, there has been considerable interest in identifying diagnostic markers that offer specificity for AFX/PDS or are pertinent to this differential diagnosis. Recently, whole-exome sequencing analysis revealed high-level PDGFRA/B gene expression and suggested PDGFRB immunohistochemistry (IHC) as a "lineage specific" marker for PDS. To evaluate the potential diagnostic utility of PDGFRB status, we examined CD140b (PDGFRB) protein expression in a well-characterized cohort of AFX, PDS, and morphologic mimics.

**Design:** Clinical information and details regarding each patient's diagnosis were collected. Formalin-fixed, paraffin-embedded sections from 15 AFX, 5 PDS, 21 squamous cell carcinomas (SCC) (8 sarcomatoid, 8 poorly differentiated, and 5 moderately differentiated), 29 melanomas (5 desmoplastic and 24 non-desmoplastic), and 6 cutaneous leiomyosarcomas were retrieved. An automated IHC system (Ventana BenchMark XT) was used for the detection of CD140b, using a commercially available antibody (RM303, 1:2000, RevMAb Biosciences). Cases were independently reviewed and scored as negative (<5%), 1+ (5%-25%), 2+ (26%-50%), or 3+ (>50%).

**Results:** The results of CD140b IHC are summarized in Table 1. All AFX and PDS were diffusely positive (20/20). CD140b IHC showed a variable extent of staining in 4/21 SCC (4/8 sarcomatoid and 0/13 poorly/moderately differentiated SCC) and 9 of 29 melanomas (5/5 desmoplastic and 4/24 non-desmoplastic). 1+ positivity was observed in 2/6 cutaneous leiomyosarcomas. In some cases, non-lesional fibroblastic stromal cells and intra-tumoral vessels exhibited diffuse CD140b reactivity, complicating the interpretative analysis.

Table 1. Summary of CD140b protein overexpression

Tumor type		Total cases	CD140b-positive (%)	Negative	1+	2+	3+
AFX/PDS		20	20 (100%)	0	0	0	20
	AFX	15	15 (100%)	0	0	0	15
	PDS	5	5 (100%)	0	0	0	5
SCC		21	4 (19%)	17	1	2	1
	Sarcomatoid	8	4 (50%)	4	1	2	1
	Poorly differentiated	8	0 (0%)	8	0	0	0
	Moderately differentiated	5	0 (0%)	5	0	0	0
Melanoma		29	9 (31%)	20	5	0	4
	Desmoplastic	5	5 (100%)	0	2	0	3
	Non-desmoplastic	24	4 (13.8%)	20	3	0	1
Cutaneous leiomyosarcoma		6	2 (33.3%)	4	2	0	0

**Conclusions:** In a practical sense, although CD140b may not be truly lineage specific, it does show utility as a diagnostic marker of AFX and PDS. Notably, CD140b expression also correlates with desmoplastic component in melanoma and is expressed in a subset of sarcomatoid SCC. Several targeted drugs have shown efficacy in PDGFR-expressing tumors, and our findings further delineate therapeutic strategies for a selected group of cutaneous sarcomatoid neoplasms.

**421 Characterizing Infection-Related IgA Vasculitis in the Skin**Jodi Gedalovich<sup>1</sup>, Ksenia Kasimova<sup>2</sup>, Zhengchun Lu<sup>3</sup>, Vanderlene Kung<sup>3</sup>, Ryanne Brown<sup>2</sup>, Megan Troxell<sup>4</sup><sup>1</sup>Stanford Health Care, Palo Alto, CA, <sup>2</sup>Stanford Medicine/Stanford University, Stanford, CA, <sup>3</sup>Oregon Health & Science University, Portland, OR, <sup>4</sup>Stanford University Medical Center, Stanford, CA

**Disclosures:** Jodi Gedalovich: None; Ksenia Kasimova: None; Zhengchun Lu: None; Vanderlene Kung: None; Ryanne Brown: None; Megan Troxell: None

**Background:** Cutaneous vasculitis with IgA deposition (clgAV) is most closely associated with Henoch-Schonlein Purpura (HSP, currently termed systemic IgA vasculitis). This syndrome classically presents as abdominal pain, joint pain, IgA nephropathy, and/or skin lesions in a child, sometimes after an upper respiratory infection. There is a growing literature on IgA-dominant infection-related glomerulonephritis (IGRN) in older adults, particularly related to *Staphylococcus* infections in diabetic adults. In analogy, we aimed to study the frequency of clgAV, as well as the types of infections, pathogenic organisms, clinical presentations, and direct immunofluorescence (DIF) characteristics associated with these cases.

**Design:** We searched our pathology database for direct immunofluorescence-detected vascular-perivascular IgA deposits present on skin biopsy at our institution from 2017-2022. Patients older than 18 years of age with accessible electronic medical records were eligible for inclusion. Retrospective chart review for demographic information, clinical presentation descriptions, laboratory data, and pathology reports was performed.

**Results:** In our cohort of 43 patients, dermatologists consistently described the skin lesions as non-blanching and erythematous macules, papules, or petechiae with involvement of the lower extremities in all 43 patients. Seventeen patients (43%) were found to have a bacterial or fungal infection within 6 months of their initial diagnosis of clgAV. Diabetes was infrequent in the cohort (18.6%) but was nearly five times more common in those with infection (35.3 vs 7.7%). *Staphylococcus aureus* was the most frequently implicated pathogen (23.5%) and skin and soft tissue infections were most commonly reported (41.2% of those with one infection, up to 53% considering multiple infections). DIF demonstrated that patients with infections tended to have higher intensity IgA, C3, and fibrinogen deposition.

		No infection	Infection
Patients (#, %)		26 (57)	17 (43)
Sex (n, %)	Male	14 (53.8)	7 (41.2)
	Female	12 (46.2)	10 (58.8)
Average age, years (range)**		41 (21 - 78)	51 (21 - 75)
Diabetes**		2 (7.7)	6 (35.3)
Abnormal creatinine (#, %) n = 18, 17		3 (11.5)	7 (41.2)
Hematuria (n, %)		12 (57.1)	10 (71.4)
Abnormal C3 (#, %) n = 10, 9		0 (0)	1 (11.1)
Leukocytoclastic vasculitis		24 (92.3)	15 (88.2)
IgA DIF (n, %)**	0 – 1+	24 (92.3)	10 (58.8)
	2 – 3+	2 (7.7)	7 (41.2)
C3 DIF (n, %)	Absent (0)	9 (34.6)	4 (23.5)
	Present (1– 3+)	18 (66.4)	13 (76.5)
Organisms (# infections)			Staphylococcus aureus - 4 Group A Streptococcus - 3 Corynebacterium striatum - 2 Clostridioides difficile - 1 Gram negative bacteria - 5 Pseudallescheria boydii - 1 Unidentified - 2

Demographics, laboratory data, and immunofluorescence by group (\*\*p-value <0.05)

**Conclusions:** In our experience, a significant fraction (43%) of adult cutaneous IgA vasculitis cases are associated with bacterial or fungal infections. As reported with IGRN, *S. aureus* was a frequently implicated pathogen. The association of clgAV with not only Henoch-Schonlein Purpura but also infection is of critical importance to recognize, as the treatment differs. Pathologists and clinicians should carefully rule out infection before administering immunosuppression for IgA vasculitis.

## 422 Investigation of NPM1 Mutation Frequency in Cutaneous Blastic Plasmacytoid Dendritic Cell Neoplasms

Hanan Hamdan<sup>1</sup>, Weina Chen<sup>1</sup>, Miguel Cantu<sup>1</sup>, Sharon Koorse Germans<sup>1</sup>, Franklin Fuda<sup>1</sup>, Alexa Siddon<sup>2</sup>, Adam Bagg<sup>3</sup>, Robert Hasserjian<sup>4</sup>, Maximiliano Ramia de Cap<sup>5</sup>, Mingyi Chen<sup>1</sup>, Travis Vandergriff<sup>1</sup>, Olga Weinberg<sup>1</sup>

<sup>1</sup>UT Southwestern Medical Center, Dallas, TX, <sup>2</sup>Yale School of Medicine, New Haven, CT, <sup>3</sup>University of Pennsylvania, Philadelphia, PA, <sup>4</sup>Massachusetts General Hospital, Harvard Medical School, Boston, MA, <sup>5</sup>North Bristol NHS Trust, Bristol, United Kingdom

**Disclosures:** Hanan Hamdan: None; Weina Chen: None; Miguel Cantu: None; Sharon Koorse Germans: None; Franklin Fuda: None; Alexa Siddon: None; Adam Bagg: None; Robert Hasserjian: None; Maximiliano Ramia de Cap: None; Mingyi Chen: None; Travis Vandergriff: None; Olga Weinberg: None

**Background:** Background: Acute myeloid leukemia (AML) and blastic plasmacytoid dendritic cell neoplasm (BPDCN) show clinicopathological overlapping presentations, which makes them challenging to differentiate on a small skin biopsy. NPM1 mutations are the most common genetic lesions in AML, accounting for one third of cases and cause an aberrant cytoplasmic delocalization of NPM1 protein mutants, which can be detected by an immunohistochemical stain (IHC). The frequency of NPM1 mutations in BPDCN remains controversial, but different studies showed frequencies of 15-29% in MS patients [1]. We aimed to investigate BPDCN cases for NPM1 mutations and compare them with cutaneous NPM1 positive leukemia cutis cases.

**Design:** Aim: To show that the cytoplasmic expression of nucleophosmin by immunohistochemistry can be used to differentiate between BPDCN and cutaneous NPM1 positive myeloid sarcoma. Methods: From a multi-institutional search, we identified and analyzed a total of 8 cases of cutaneous BPDCN and 19 cases of *NPM1*-mutated cutaneous myeloid sarcoma (7 of which were primary leukemia cutis). The IHC antibody detects A, B, and D subtypes of *NPM1* mutations that account for ~90% of mutation subtypes. We compared the clinical and pathological findings of these patients and identified distinguishing features between these groups.

**Results:** Results: BPDCN patients presented at an older age, had lower WBC, higher hemoglobin level, and higher platelets counts than cutaneous myeloid sarcoma patients ( $p < 0.05$ ; Table 1). The bone marrow of patients in both groups was similarly involved at the time of diagnosis with no significant difference; however, the percentage of involvement was significantly different among the two groups (Table 1). Overall and event-free survival rates were not significantly different among the two groups. Next-generation sequencing profile differed among the two groups, with a significant enrichment of NPM1 in cutaneous myeloid sarcoma, while no NPM1 mutation was detected by NGS or immunohistochemistry (IHC) in BPDCN cases.

Table-1: Comparison of clinical presenting characteristics of Blastic Plasmacytoid Dendritic Neoplasm vs cutaneous Myeloid sarcoma cases. Values with asterisks are significant at  $p < 0.05$ .

	Blastic Plasmacytoid Dendritic Neoplasm cases	Cutaneous Myeloid sarcoma cases	P value
Total	N=8	N=19	
Age: Mean (range)	74 (66-83) *	62 (41-77) *	0.0011
Gender	M=7; F=1	M=11; F=8	
WBC at diagnosis: Mean; SD	6.7 (4.3) *	15.2 (15.3) *	0.0401
Hgb: Mean	12.5 *	9.9 *	0.0312
Platelets: Mean	246 *	125 *	0.0091
BM involvement at diagnosis	62.5 (5/8)	63.1 (12/19)	p> 0.5
BM involvement by disease	34.4	56.21	p> 0.5
BM cellularity	59.29	70.33	p> 0.5
NPM1 IHC positivity	None	19/19 (100%)	
Median survival (months)	18.5	190.5	
Overall survival, HR (95% CI)	1.03 (0.3914 to 2.709)		
Event-Free Survival (95% CI)	0.7367 (0.2268 to 2.560)		

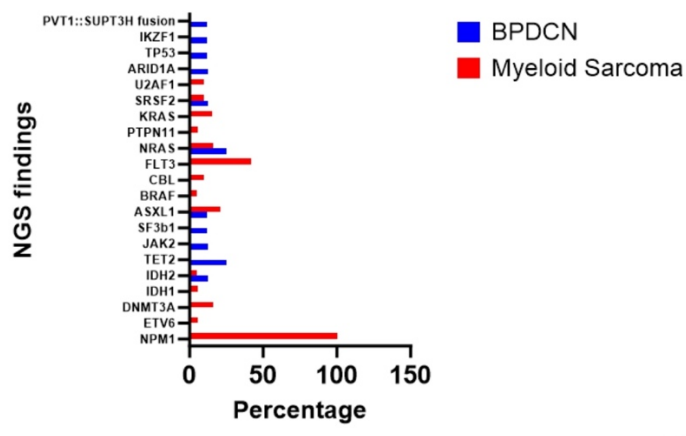
Abbreviations: IHC: Immunohistochemistry, HR: Hazard Ratio, CI: Confidence interval.

## ABSTRACTS | DERMATOPATHOLOGY

Table-2: Comparison of cytogenetics and molecular findings of Blastic Plasmacytoid Dendritic Neoplasm vs cutaneous myeloid sarcoma cases. Values with asterisks are significant at  $p < 0.05$ . All  $p$  values  $<0.05$ .

Molecular Findings (%)	Blastic Plasmacytoid Dendritic Neoplasm cases	Cutaneous Myeloid sarcoma cases
Complex Karyotype (%)	37.5 (3/8)	15.7 (3/19)
<i>NPM1</i>	(0/8)	100 (19/19)
<i>ETV6</i>	ND	5.3 (1/19)
<i>DNMT3A</i>	ND	15.7 (3/19)
<i>IDH1</i>	ND	5.3 (1/19)
<i>IDH2</i>	12.5 (1/8) *	5.3 (1/19)
<i>TET2</i>	25 (2/8)	ND
<i>JAK2</i>	12.5 (1/8)	ND
<i>SF3b1</i>	12.5 (1/8)	ND
<i>ASXL1</i>	12.5 (1/8) *	21 (4/19)
<i>BRAF</i>	ND	5.3 (1/19)
<i>CBL</i>	ND	10.5 (2/19)
<i>FLT3</i>	ND	42 (8/19)
<i>NRAS</i>	25 (2/8) *	15.7 (3/19)
<i>PTPN11</i>	ND	5.3 (1/19)
<i>KRAS</i>	ND	15.7 (3/19)
<i>SRSF2</i>	12.5 (1/8) *	10.5 (2/19)
<i>U2AF1</i>	ND	10.5 (2/19)
<i>ARID1A</i>	12.5 (1/8)	ND
<i>TP53</i>	12.5 (1/8)	ND
<i>IKZF1</i>	12.5 (1/8)	ND
<i>PVT1::SUPT3H fusion</i>	12.5 (1/8)	ND

Figure 1 - 422  
Molecular findings



**Conclusions:** We find that BPDCN patients present similarly to cutaneous AML patients, but lack *NPM1* mutations. *NPM1* immunohistochemical stain can be useful in the differential diagnosis of BPDCN and cutaneous myeloid sarcoma, as its abnormal expression appears to exclude BPDCN in a rapid and cost-effective manner.

### 423 Clinicopathologic and Molecular Characterization of Primary Anorectal Melanoma

Ashley Hein<sup>1</sup>, Shereen Zia<sup>1</sup>, Julie Youngs<sup>1</sup>, Scott Lauer<sup>1</sup>, Dominick DiMaio<sup>1</sup>, Joseph Khoury<sup>1</sup>, Dinesh Pradhan<sup>1</sup>

<sup>1</sup>University of Nebraska Medical Center, Omaha, NE

**Disclosures:** Ashley Hein: None; Shereen Zia: None; Julie Youngs: None; Scott Lauer: None; Dominick DiMaio: None; Joseph Khoury: None; Dinesh Pradhan: None

**Background:** Anorectal melanoma (AM) is a rare, aggressive melanoma with a 5 year survival rate of 14-30% and a distinct genetic profile. There is no standard staging system and limited consensus on optimal treatment. Immune checkpoint inhibitors

## ABSTRACTS | DERMATOPATHOLOGY

have shown a significant survival advantage in patients with stage IV melanomas, however limited AM cases were studied. Additional research is imperative to elucidate molecular pathways and find predictive biomarkers and pinpoint therapeutic targets.

**Design:** After IRB approval, 30 patients with primary AM were identified by pathology database review over a period of 33 years and their clinicopathologic, molecular, and survival information was evaluated.

**Results:** The median patient age was 69 years (range: 32-91) with a M:F ratio of 1:1.5. Tumor distribution included 18 rectal, 9 anal, and 3 anorectal cases, with an average tumor size of 15.6 mm (range: 1.35-58 mm). Of 20 patients with reported race, 84.2% were Caucasian, 5.3% Hispanic, 5.3% African American, and 5.3% Arabic. The most common presenting symptoms were rectal bleeding, anorectal mass, and weight loss. Next generation sequencing (NGS) with a 50-gene panel was performed on 7 (23.3%) patients, revealing alterations in *KIT* (4 pts), *NRAS* (2 pts), and *SF3B1* (1 pt) (Table 1). Two patients had *CDKN2A* loss. Interestingly, mutations involving *BRAF* or *NF1* genes were absent. While *KIT*, *SF3B1*, and *NRAS* mutations have been reported, to our knowledge these are the first reports of *CDKN2A* loss in AM. *CDKN2A* inactivation has previously shown to increase sensitivity to CDK4/6 inhibitors in melanoma cell lines, suggesting potential therapeutic significance. Of 24 patients with follow-up, 5 (21%) developed regional metastasis and 16 (67%) distant metastases including lung (n=2; M1b), viscera (n=11; M1c), and brain (n=3; M1d), according to AJCC 8th edition cutaneous melanoma staging system. 12 (50%) patients died, 10 (42%) were alive with disease, and 2 (8%) were disease free at last follow-up (median follow-up 22.5 mo). The 5-year survival rate was 28.6%. However, cases in which NGS was done in our study had a 0% 5-year survival. Two patients with identical *NRAS* alterations had divergent outcomes: One underwent treatment with local excision, radiation, and nivolumab and survived 20 mo, while the other went untreated and only survived for 58 days.

Table 1: Clinicopathologic Features of Anorectal Melanomas with Molecular Alterations.

	Age	Sex	Tumor Size (cm)	Nodes at Diagnosis	Stage at diagnosis	Molecular Alteration	Treatment	Status	Length of Survival (months)	Eventual Metastatic location
Case #1	91	F	5.5	Uninvolved	IV	<i>KIT</i> (W557C)	None	DOD	1	Lung, Liver, Bone, Large Bowel
Case #2	64	F	5.8	Enlarged	IIIB	<i>KIT</i> (V560G) <i>CDKN2A</i> loss	Local Excision Chemotherapy Radiation  Imatinib	DOD	26.5	Lung, Brain
Case #3	85	F	3.4	Uninvolved	IIIC	<i>NRAS</i> (Q61R)	Local Excision Radiation Nivolumab	AWD	20	NA
Case #4	54	M	1.5	Involved Inguinal LN	IIIC	<i>NRAS</i> (Q61R)	None	DOU	2	Groin
Case #5	69	F	0.46	Uninvolved	IIIC	<i>KIT</i> (L576P)	Local Excision	DOU	22.5	Lung
Case #6	79	F	0.5	Uninvolved	IIIC	<i>KIT</i> (V560D)	Local Excision Imatinib	DOU	72.5	Brain
Case #7	42	F	0.3	Uninvolved	IIA	<i>CDKN2A</i> loss <i>SF3B1</i> (R625C)	Local Excision Chemotherapy Radiation	DOD	79	Liver

NA: Not applicable, UK: Unknown, AWD: Alive with disease, DOD: Died of disease, DOU: Died of unknown cause

**Conclusions:** These findings further emphasize the aggressive nature of AM and the important role of molecular profiling in guiding therapeutic choices to improve survival.

**424 STAT6 Expression in Sebaceous Neoplasms and Mimickers**Haya Homsi<sup>1</sup>, Jennifer Ko<sup>1</sup>, Steven Billings<sup>1</sup>, Shira Ronen<sup>1</sup><sup>1</sup>Cleveland Clinic, Cleveland, OH**Disclosures:** Haya Homsi: None; Jennifer Ko: None; Steven Billings: None; Shira Ronen: None

**Background:** STAT6 is a transcription factor that belongs to the signal transducer and activator of transcription (STAT) family with a critical role in cellular proliferation. It is a highly sensitive and specific immunohistochemical nuclear marker for solitary fibrous tumor. Recently, we noticed cytoplasmic staining with a vesicular pattern for STAT6 in sebaceous glands of normal skin. The aim of this study was to evaluate STAT6 staining patterns in various sebaceous neoplasms and mimickers.

**Design:** We examined STAT6 expression in various sebaceous lesions, including 9 sebaceous adenomas, 4 sebaceomas, and 18 sebaceous carcinomas, and their cutaneous mimickers, including 5 trichilemmomas, 9 hidradenomas, 6 squamous cell carcinomas (SCC), 7 basal cell carcinomas (BCC), 5 metastatic renal cell carcinomas (RCC), and 8 Merkel cell carcinomas (MCC).

**Results:** STAT6 was expressed in 9/9 (100%) sebaceous adenomas, 4/4 (100%) sebaceomas, 18/18 (100%) sebaceous carcinomas, 2/9 hidradenomas, 5/5 (100%) metastatic RCC, and 6/8 (75%) MCC. The staining pattern observed in the sebaceous neoplasms showed a distinctive cytoplasmic and membranous vesicular (small vesicles) pattern. The hidradenomas and MCC mostly exhibited granular cytoplasmic staining. The surrounding normal tissue was negative. STAT6 expression was not seen in trichilemmomas, SCC, and BCC.

Figure 1 - 424

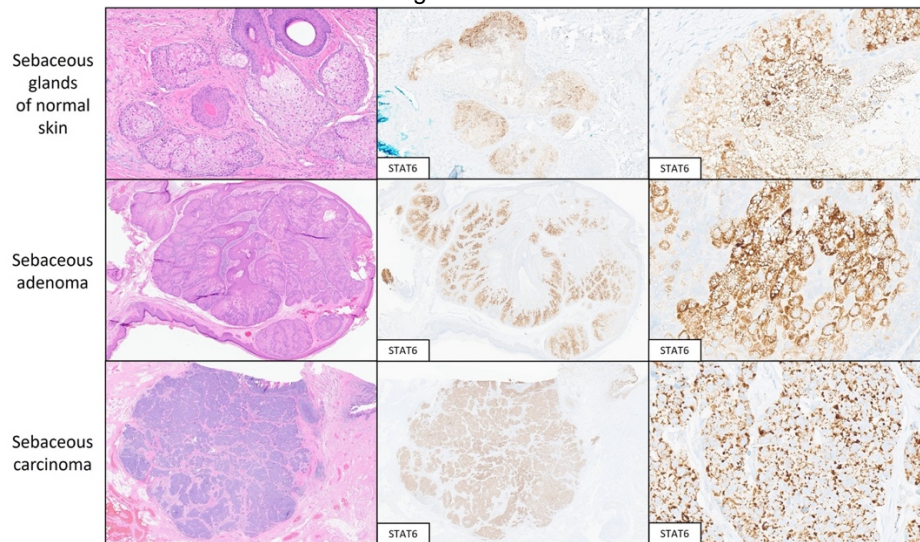
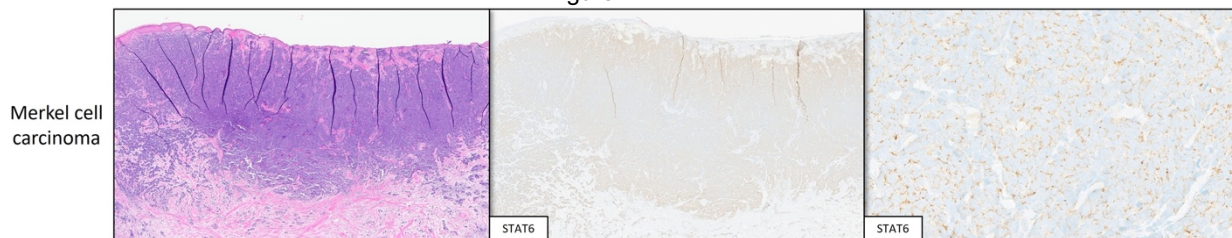


Figure 2 - 424



**Conclusions:** Our findings suggest that use of STAT6 can be helpful for identifying intracytoplasmic lipids, as seen in sebaceous neoplasms and renal cell carcinomas, thereby offering diagnostic utility for identifying sebaceous differentiation in primary skin tumors. Notably, the expression pattern of STAT6 was akin to the pattern of adipophilin stain, and differs significantly from that of MCC and hidradenomas, which exhibit granular staining, as opposed to intracytoplasmic small vesicles seen in sebaceous neoplasms. The broader application of STAT6 as a marker for sebaceous lesions necessitates further validation through comprehensive and larger-scale studies.

**425 The Clinicopathological and Prognostic Features of Promoter Mutation, Rs2853669 Polymorphism and Methylation within the TERT Gene in Chinese Melanoma Patients**

Jue Hu<sup>1</sup>, Xu Cai<sup>2</sup>, Yunyi Kong<sup>2</sup>

<sup>1</sup>Fudan University Shanghai Cancer Center, Shanghai Medical College, Fudan University, Shanghai, China, <sup>2</sup>Fudan University Shanghai Cancer Center, Shanghai, China

**Disclosures:** Jue Hu: None; Xu Cai: None; Yunyi Kong: None

**Background:** Telomerase reverse transcriptase (TERT) gene promoter mutations in Chinese melanoma patients remained to be studied. The status of single nucleotide polymorphism (SNP) site rs2853669 and methylation level of TERT promoter in Chinese melanoma patients were also not unveiled.

**Design:** Sanger sequencing was used to detect the mutation of TERT gene promoter region, the status of rs2853669 and the BRAF hotspot mutation in 93 cases of primary melanoma. Pyrosequencing was used to detect the methylation level of 5 CpG sites, located in upstream of transcription start site (UTSS region) of TERT gene, in primary tumor tissues of 15 melanoma patients as well as their paired normal skin and subsequent metastatic tissues.

**Results:** Ninety-three cases of patients with primary melanoma were all Chinese, including 47 males and 46 females. The ages of patients ranged from 26 to 87 years old. 25(26.9%) cases had TERT promoter mutations. 9(36.0%) of them were -124bp C>T mutations, 3(12.0%) were -138/139bp CC>TT mutations, and 13(52.0%) were -146bp C>T mutations. These three mutation types did not coexist. 66(71.0%) cases were found to be SNP rs2853669 carriers. TERT promoter mutation was mainly found in non-acral cutaneous melanoma, the mutation frequency of which was 43.5% (20/43). But it less frequently mutated in acral lentiginous melanoma and mucosal melanoma (5/47, 10.6%) ( $P<0.01$ ) (Table). BRAF and TERT mutations had tendency to coexist( $P<0.01$ ) (Table). In non-acral cutaneous melanoma, there was no significant association between TERT promoter and/or BRAF mutation and progression-free survival (PFS), but the PFS of patients with TERT promoter and/or BRAF mutation tended to be shorter than those with wild-type (Figure A-C). Notably, in all the patients, the PFS of rs2853669 carriers tended to have longer survival than non-carriers, though there was still no statistically significance (Figure D). Pyrosequencing was performed in 15 patients, and 2 of them were TERT promoter mutated. The methylation level of TERT promoter UTSS region in primary and metastatic tumors is generally higher than those in normal tissues (Figure E-F). Interestingly, taking the mean methylation level of the normal group as the threshold value, the primary lesions were divided into hypermethylation group and hypomethylation group. All of the 2 cases with TERT mutation were found to be hypomethylated.

Correlation of TERT promoter mutation with tumor subtype and BRAF hotspot mutation

	TERT mutation (N=25)	TERT wild type (N=68)	P value
<b>Subtype</b>			<0.01
Non-acral cutaneous	20 (43.5%)	26 (56.5%)	
SSM	17	23	
NM	2	3	
LMM	1	0	
Acral and mucosal	5 (10.6%)	42 (89.4%)	
ALM	3	34	
MM	2	8	
<b>BRAF</b>			<0.01
Mutation	15 (45.5%)	18 (54.5%)	
Wild type	10 (16.7%)	50 (83.3%)	

SSM: Superficial spreading melanoma; NM: Nodular melanoma; LM: Lentigo maligna melanoma; ALM: Acral lentiginous melanoma; MM: Mucosal melanoma

Figure 1 - 425

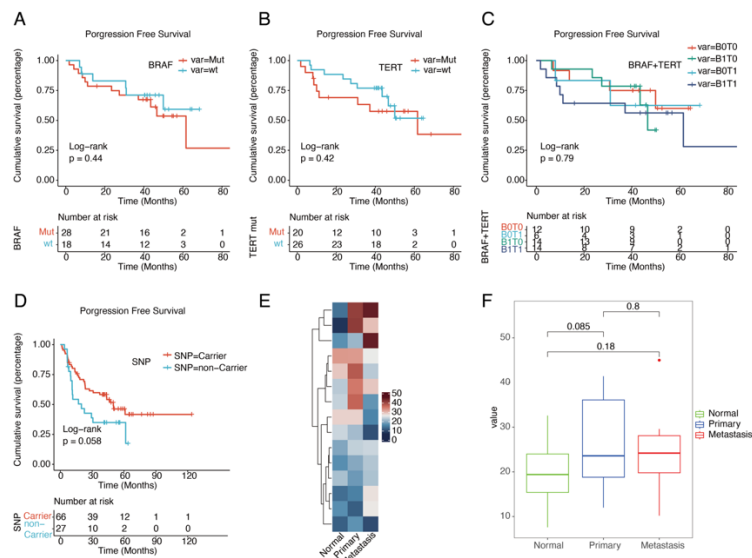


Figure A. Kaplan-Meier curve of TERT promoter mutation for PFS of non-acral cutaneous melanoma; B. Kaplan-Meier curve of BRAF hotspot mutation for PFS of non-acral cutaneous melanoma; C. Kaplan-Meier curve of TERT promoter mutation and BRAF hotspot mutation for PFS of non-acral cutaneous melanoma. D. Kaplan-Meier curve of TERT promoter SNP rs2853669 for PFS of non-acral cutaneous melanoma. E. Heatmap of methylation level in 15 examples of paired normal tissue, primary melanoma, and metastatic melanoma. F. Boxplot of methylation level in 15 examples of paired normal tissue, primary melanoma, and metastatic melanoma.

**Conclusions:** TERT promoter more frequently mutated in non-acral cutaneous melanoma than in acral and mucosal melanoma. TERT promoter mutation prefers to coexist with BRAF hotspot mutation, and single or dual gene mutations may indicate a shorter PFS. SNP rs2853669 carrier may be a favorable factor for PFS. TERT promoter showed hypermethylation in primary and metastatic melanoma without TERT promoter mutation.

## 426 Clinicopathological, Fluorescence In-situ Hybridization and Prognostic Features of Nevoid Melanoma

Jue Hu<sup>1</sup>, Min Ren<sup>2</sup>, Xu Cai<sup>2</sup>, Yunyi Kong<sup>2</sup>

<sup>1</sup>Fudan University Shanghai Cancer Center, Shanghai Medical College, Fudan University, Shanghai, China, <sup>2</sup>Fudan University Shanghai Cancer Center, Shanghai, China

**Disclosures:** Jue Hu: None; Min Ren: None; Xu Cai: None; Yunyi Kong: None

**Background:** Nevoid melanoma (NeM) is a rare subtype of melanoma that resembles common nevus in low power silhouette, and likely to be wrongly diagnosed. NeM in Asian population is still remained to be explored.

**Design:** Twenty-four cases of NeM were collected in Fudan University Shanghai Cancer Center from 2018 to 2023. The clinicopathological characteristics and follow-up data were retrospectively analyzed. The Vysis Melanoma FISH probe kit, combined with 9p21(INK4a) and 8q24(MYC) assays were performed in all patients.

**Results:** We identified 24 cases of nevoid melanoma from 24 patients (6 males and 18 females). Fifteen cases were classified as papillomatous NeM. The age of the patients ranged from 11 to 60 years old (mean=34). This group resembling papillomatous dermal nevi had a mean Breslow thickness of 2.2 mm (range 0.8-4.5mm). Junctional melanocytes were only focal or complete absent. Impaired maturation was observed in 80% (12/15) cases. Mitotic figures ranged from 1 to 11/mm<sup>2</sup> (mean=4/mm<sup>2</sup>) and could be found in deeper portion in 11 cases. At the time of diagnosis, 5 patients had local-regional lymph node metastasis. Non-papillomatous NeM comprised 9 patients. The average age of this group was 40(range 22 to 59 years old). This group was flat or slightly dome shaped. The mean Breslow thickness was 1.5mm (range 0.5-2.6mm). Junctional proliferation of atypical melanocytes could be observed in 7 cases. Impaired maturation was present in 7 cases. Mitotic figures ranged from 1 to 2/mm<sup>2</sup> (mean=1/mm<sup>2</sup>). Deep dermal mitosis presented in 4 cases. Immunohistochemically, 21/21(100%), 12/20 (60%) and 3/21 (14.3%) showed diffusely positive for SOX10, MelanA and HMB45, respectively. But there were 8/20 (40%) and 18/21 (85.7%) showed a diminished expression pattern for MelanA and HMB45 with the increasing depth. Ki-67 was higher in the superficial component compared with the deeper component. FISH studies were positive in 83.3% (20/24) of the cases studied, including 13 papillomatous NeM (86.7%)

## ABSTRACTS | DERMATOPATHOLOGY

and 7 non-papillomatous NeM (77.8%). CCND1 gain demonstrated the highest proportion of positive cases (15/24, 62.5%). The follow-up time ranged from 3 to 100 months (median=34.0months). 21 patients had no evidence of disease. 3 patients had distant metastasis, one of them eventually died from melanoma, and these three patients were all papillomatous NeM.

**Conclusions:** FISH assay is a valuable adjunct for the diagnosis of NeM. Papillomatous NeM may have poorer outcome than non-papillomatous NeM.

### 427 Pathological Parameter for Anti-PD-1 Therapy Response Evaluation of Melanoma in Asians

Tao Jiao<sup>1</sup>, Qian Guo<sup>1</sup>, Haizhen Du<sup>1</sup>, Xia Liu<sup>2</sup>, Hongzhe Sun<sup>2</sup>, Shuo Han<sup>2</sup>, Lin Zhu<sup>2</sup>, Zhifu Zhang<sup>2</sup>, Na Li<sup>2</sup>, Yan Kong<sup>1</sup>

<sup>1</sup>Peking University Cancer Hospital, Beijing, China, <sup>2</sup>Beijing PhenoVision Bio Co., Ltd., Beijing, China

**Disclosures:** Tao Jiao: None; Qian Guo: None; Haizhen Du: None; Xia Liu: None; Hongzhe Sun: None; Shuo Han: None; Lin Zhu: None; Zhifu Zhang: None; Na Li: None; Yan Kong: None

**Background:** Melanoma is the deadliest form of skin cancer. Although immune checkpoint inhibitors, such as anti PD-1 and anti-PD-L1 therapies have exhibited significant survival improvement in advanced melanoma, many Asian patients do not benefit from these therapies due to high ratio of acral and mucosal melanoma subtypes. Tumor microenvironment has demonstrated its importance of identify appropriate patients for immunotherapies in a variety of cancers. Current study aimed to find pathological parameters with correlation of anti PD-1 therapy response in Asian melanoma patients.

**Design:** Twenty-four melanoma cases received PD-1 monoclonal antibody immunotherapy in our hospital were evaluated in current study. Among them, 11 cases exhibited a partial response (PR) including four acral, two mucosal and five cutaneous subtypes, and 13 cases were progressive disease (PD), with seven acral, two mucosal and four cutaneous melanomas, respectively. Median PFS in PR group and in PD group were 25 and 3 months, respectively. Archived patient FFPE sections were examined utilizing multiplex immunofluorescence staining with PN 6-Plex Detection Kit (PhenoVision Bio Co., Ltd) targeted CD68, CD3, CD20, S100, PD-L1 and PD-1. The multiple staining images were scanned, tumor areas were lined out by pathologists and analyzed using Oncotopix Discovery system (Visiopharm). The positive cell numbers of CD3, CD20, CD68, PD-1+CD68, PD-1+CD3, PD-1+CD20, PD-L1+CD68, PD-L1+CD3, PD-L1+CD20, PD-L1+S100, and others (any other cell) were calculated. Spatial analysis was examined by setting each S100 positive cell as center to count other cell types from 0-25, 25-50 and 50-100 micrometers ( $\mu$ m) of center cells.

**Results:** The positive cell ratios of CD68, CD3, CD20, PD-L1, and PD-1 in PR group and PD group were 2.94%, 6.04%, 2.85%, 1.34%, 0.34% and 0.74%, 4.47%, 1.24%, 0.41%, 0.04%, respectively. CD3/PD-1 co-positive cell ratio was significantly higher in PR group than in PD group,  $p = 0.04$ . The spatial analysis exhibited significant higher of CD3/PD-1 co-positive cell ratio within 25-50  $\mu$ m of tumor cells in PR group compared to PD group ( $p=0.028$ ). According to the ROC curves generated from clinical response data, the response score AUC of PD-1/CD3 co-positive was 0.881 (95% CI: 0.722-1.0).

**Conclusions:** Current results indicate that PD-1/CD3 co-positive may be a valuable pathological parameter for anti-PD-1 therapy response of melanoma in Asians.

### 428 Identification of Novel Fusions in Melanoma by Next-Generation Sequencing: A Retrospective Analysis of 144 Patients from a Single Tertiary Cancer Center

Moon Joo Kim<sup>1</sup>, Richard Yang<sup>1</sup>, Priya Nagarajan<sup>1</sup>, Phyuan Aung<sup>1</sup>, Jonathan Curry<sup>1</sup>, Woo Cheal Cho<sup>1</sup>

<sup>1</sup>The University of Texas MD Anderson Cancer Center, Houston, TX

**Disclosures:** Moon Joo Kim: None; Richard Yang: None; Priya Nagarajan: None; Phyuan Aung: None; Jonathan Curry: None; Woo Cheal Cho: None

**Background:** While gene fusions are infrequent in melanomas, those involving rearrangements in receptor tyrosine kinase genes often lack mutations in *BRAF*, *NRAS*, and *NF1* (termed triple wild-type (WT)). This supports the notion that gene rearrangements play an oncogenic role in these melanomas. Thus, identifying gene fusions may carry therapeutic implications for a subset of melanomas.

# ABSTRACTS | DERMATOPATHOLOGY

**Design:** We conducted a retrospective analysis of melanoma patients who underwent molecular testing via next-generation sequencing (NGS) at our institution between 2021 and 2023, aiming to assess the frequency and specific types of fusions in melanomas. Relevant demographic, clinicopathologic, and molecular data—such as somatic mutations, copy number variations, tumor mutational burden (TMB), and gene fusions—were documented.

**Results:** The cohort comprised 68 primary and 76 metastatic melanomas, categorized as 106 (74%) non-acral cutaneous, 15 (10%) mucosal, 8 acral (6%), and 6 (4%) uveal/blue-nevus-like melanomas, with 9 cases (6%) of unknown primary. Overall, gene fusions were found in 4% (6/144) of melanomas (clinicopathologic and molecular profiles summarized in Figure 1). Patients with gene fusions had a 1:1 male-to-female ratio and a median age of 65.5 years (range: 19-75 years). Among the fusion-associated melanomas, 67% (4/6) were non-acral cutaneous, while the rest were mucosal (anorectal and vaginal). *BCR* (n=2) (Figure 2) and *BRAF* (n=2) fusions were most common, followed by *ALK* (n=1) and *TMPRSS2* (n=1) fusions. Notably, fusions involving *BRAF* and *TMPRSS2* genes were found to be intragenic fusions. Mutations in *BRAF*, *NRAS*, or *NF1* were seen in 33% (2/6) of fusion-associated melanomas, one with a *BRAF* missense mutation (c.1790T>A, p.L597Q). Half of the melanomas with fusion transcripts harbored *TERT* promoter mutations (TPMs), and 67% (4/6) exhibited a low TMB (<5 mut/Mb).

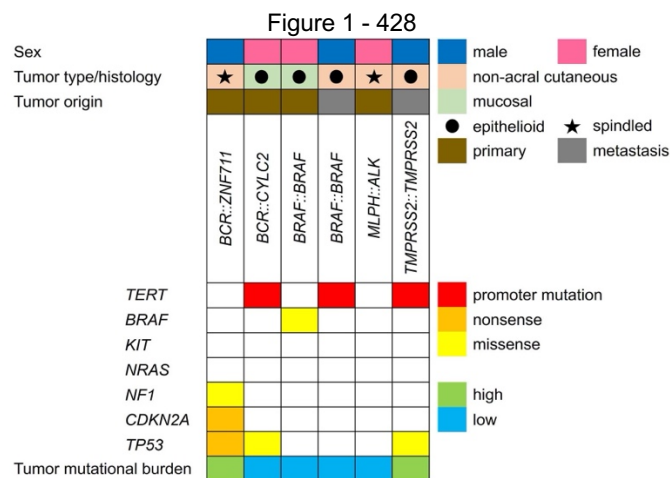
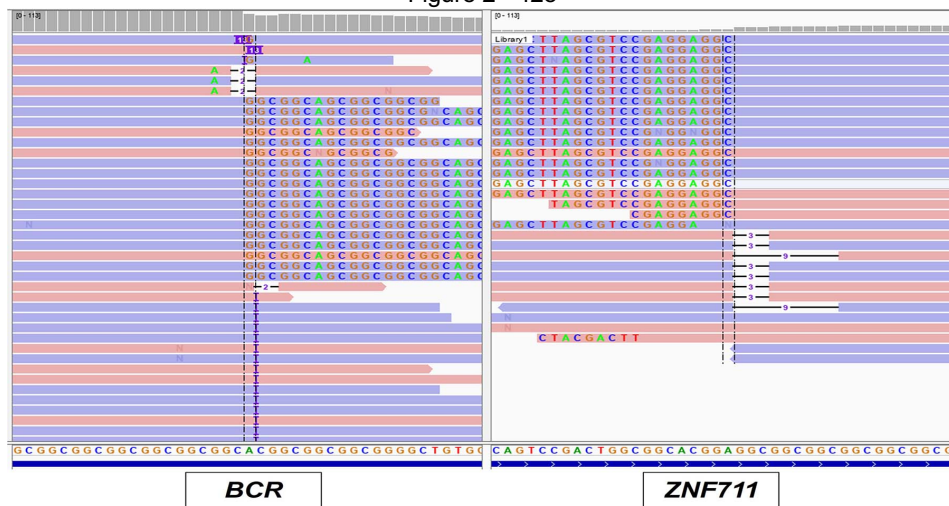


Figure 2 - 428



An example of melanoma with *BCR*::*ZNF711* fusion. Intronic fusion breakpoints of the *BCR* and *ZNF711* genes as shown in IgV (Integrated Genomic Viewer v2.7.0). The left panel shows an upstream genomic fusion breakpoint within intron 1 (chr22:23,522,769) of the *BCR* gene (genomic coordinates chr22:23,522,759-23,522,799 from hg19 [human genome 19]). The right panel shows the corresponding downstream genomic fusion breakpoint within the 5' untranslated region (chrX:84,499,139) of the *ZNF711* gene (genomic coordinates chrX:84,499,068-84,499,190). Genomic coordinates are from Genome Reference Consortium Human Build 37 (GRCh37).

**Conclusions:** Through NGS, we identified 3 novel fusions, including 1 intragenic fusion, which have not been previously documented in melanoma: *BCR::ZNF11*, *BCR::CYLC2*, and *TMPRSS2::TMPRSS2*. *BCR* fusions in solid tumors are exceedingly rare, only having been documented in a subset of breast carcinomas and oropharyngeal squamous cell carcinoma. *TMPRSS2* fusions have predominantly been linked to prostate cancer. Our study indicates that fusion-associated melanomas are often triple WT, with low TMB, displaying ultraviolet signatures with TPMs. Further studies with a larger cohort are warranted to validate these observations.

#### 429 TRPS1 Expression is Frequently Seen in a Subset of Cutaneous Mesenchymal Neoplasms and Tumors of Uncertain Differentiation: A Potential Diagnostic Pitfall

Moon Joo Kim<sup>1</sup>, Yi Liu<sup>2</sup>, Woo Cheal Cho<sup>1</sup>

<sup>1</sup>The University of Texas MD Anderson Cancer Center, Houston, TX, <sup>2</sup>Royal Columbian Hospital, University of British Columbia, New Westminster, BC

**Disclosures:** Moon Joo Kim: None; Yi Liu: None; Woo Cheal Cho: None

**Background:** TRPS1 immunohistochemistry (IHC) was initially regarded as a highly sensitive and specific marker for mammary carcinomas and mesenchymal tumors. However, recent data challenges this notion, indicating that TRPS1 expression is not exclusive to breast neoplasms. It has been observed in various cutaneous epithelial neoplasms, including extramammary Paget disease, squamous cell carcinoma in situ, and certain adnexal neoplasms. Nonetheless, data on TRPS1 expression in cutaneous mesenchymal neoplasms and tumors of uncertain differentiation (CMNTUD) remain limited.

**Design:** We collected cases of dermatofibrosarcoma protuberans (DFSP) (n=20), dermatofibroma (DF) (n=22), cutaneous leiomyosarcoma (n=8), leiomyoma (n=8), angiosarcoma (n=19), Kaposi sarcoma (KS) (n=5), neurofibroma (NF) (n=17), and atypical fibroxanthoma (AFX) (n=20). Selected cases were subjected to immunohistochemical analysis using anti-TRPS1 antibody (Abcam, EPR16171, 1:2000). H-scores were calculated for each case by multiplying the intensity (0=none, 1=weak, 2=moderate, 3=strong) and extent (0-100) of TRPS1 expression. H-scores were compared between groups via two-tailed t-test.

**Results:** The IHC findings are summarized in Figure 1. TRPS1 expression was common in DFs (100%; 22/22), leiomyomas (100%; 8/8), AFXs (95%; 19/20), leiomyosarcomas (75%; 6/8), and DFSPs (60%; 12/20), with AFXs having the highest median H-score of 240 (Figure 1 and Figure 2). TRPS1 expression was rare in angiosarcomas and KSs. In AFXs, when present, it was mostly diffuse (84%; 16/19) and at least moderate (89%; 17/19). The H-scores of AFXs were significantly higher than those of leiomyosarcomas, a morphological differential diagnosis of AFX ( $p=0.03$ ). The difference between DFSPs and DFs in H-score was highly significant ( $p<0.0001$ ), while leiomyosarcomas and leiomyomas showed no statistically significant difference ( $p=0.32$ ).

Figure 1 - 429

Figure 1. TRPS1 expression frequency and median H-score by tumor type		
	TRPS1 expression frequency*	Median H-score
AFX (n=20)	19/20 (95%)	240
Angiosarcoma (n=19)	2/19 (11%)	0
Kaposi sarcoma (n=5)	1/5 (20%)	0
Dermatofibroma (n=22)	22/22 (100%)	140
DFSP (n=20)	12/20 (60%)	10
Neurofibroma (n=17)	4/17 (24%)	0
Leiomyosarcoma (n=8)	6/8 (75%)	85
Leiomyoma (n=8)	8/8 (100%)	170

All positive cases showed nuclear expression of TRPS1  
 Abbreviations: TRPS1, trichorhinophalangeal syndrome type 1; AFX, atypical fibroxanthoma; DFSP, dermatofibrosarcoma protuberans

Figure 2 - 429

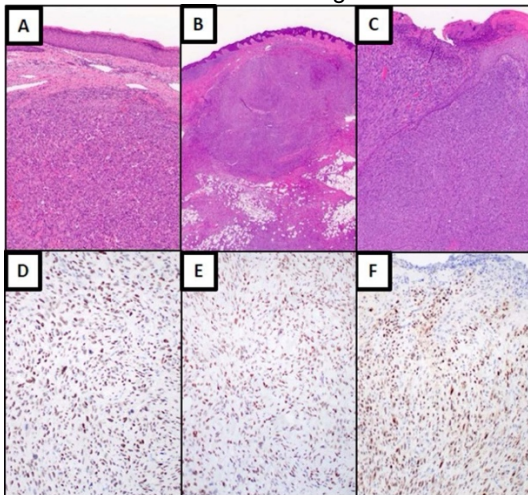


Figure 2.  
Representative cases of atypical fibroxanthoma (A: H&E, 4 x, D: TRPS1, 10 x), dermatofibrosarcoma protuberans (B: H&E, 1 x, E: TRPS1, 10 x), and leiomyosarcoma (C: H&E, 4 x, F: TRPS1, 10 x) showing diffuse and strong expression of TRPS1.

Abbreviations: H&E, hematoxylin and eosin; TRPS1, trichorhinophalangeal syndrome type 1

**Conclusions:** TRPS1 exhibits variable expression in CMNTUD, with AFXs showing the highest immunoreactivity. This underscores that TRPS1 expression is not confined to tumors of breast origin, reaffirming the crucial role of interpreting IHC results within the appropriate histopathologic context to avoid potential diagnostic pitfalls. Further studies with larger, more diverse CMNTUD cohorts are in process to validate these observations.

#### 430 Evaluation of Interleukin-36 Expression in Benign Acanthomas/Keratoses and Precursors of Squamous Cell Carcinoma

Andrea Krajisnik<sup>1</sup>, Neda Rezaee<sup>2</sup>, Bonnie Balzer<sup>3</sup>, Wonwoo Shon<sup>3</sup>

<sup>1</sup>Stanford University, Palo Alto, CA, <sup>2</sup>AmeriPath/Quest Diagnostics, West Hills, CA, <sup>3</sup>Cedars-Sinai Medical Center, Los Angeles, CA

**Disclosures:** Andrea Krajisnik: None; Neda Rezaee: None; Bonnie Balzer: None; Wonwoo Shon: None

**Background:** In recent years, the Interleukin-36 (IL-36) receptor inhibitor spesolimab has emerged as an effective FDA-approved treatment for patients with generalized pustular psoriasis. Several academic dermatopathology labs have incorporated IL-36 IHC to assist in evaluating various psoriasiform dermatoses, offering insights not only for diagnosis but also potential treatment implications by targeting the Th17 pathway. During the routine evaluation of psoriasiform lesions in our practice, we have encountered high IL-36 expression in psoriasiform keratosis (PK), a distinct keratosis histologically resembling psoriasis. The clinical differential diagnosis of PK also often includes benign acanthomas/keratoses and non-melanoma skin cancers. Herein, we conducted a survey study to assess IL-36 expression in various benign acanthomas/keratoses and precursors of squamous cell carcinoma.

**Design:** Formalin-fixed, paraffin-embedded tissue sections from benign acanthomas/keratoses (19 PK, 16 seborrheic keratosis, 10 lichen planus-like keratosis, 7 clear cell acanthoma, 6 porokeratosis, and 5 each of warty dyskeratoma, acantholytic acanthoma, epidermolytic acanthoma, and melanoacanthoma) and squamous cell carcinoma precursors (12 squamous cell carcinoma in situ and 8 actinic keratosis) were obtained and immunostained for IL-36 (clone 2F4, 1:300 dilution, Cambridge, MA). The staining was scored according to the extent and intensity of staining using a numerical scale as reported previously (negative: 0, focal weak: 1+, diffuse weak: 2+, focal strong: 3+, diffuse strong: 4+).

**Results:** All 19 PKs and 7 of 16 (43.8%) seborrheic keratoses demonstrated high IL-36 expression ( $\geq 3+$ ). Of note, all IL-36 positive seborrheic keratosis cases demonstrated foci of inflamed parakeratosis with scattered neutrophils. All other keratoses/acanthomas and carcinoma precursors showed no or low IL-36 expression, apart from 1 warty dyskeratoma and 1 acantholytic acanthoma (Table 1).

Table 1. IL-36 expression in benign acanthomas/keratoses and squamous cell carcinoma precursors

	0 (negative)	1+ (focal weak)	2+ (diffuse weak)	3+ (focal strong)	4+ (diffuse strong)	Total
Psoriasisiform keratosis	0	0	0	3	16	19
Seborrheic keratosis	6	3	0	7	0	16
Lichen planus-like keratosis	3	7	0	0	0	10
Squamous cell carcinoma in situ	4	8	0	0	0	12
Actinic keratosis	6	2	0	0	0	8
Clear cell acanthoma	6	1	0	0	0	7
Porokeratosis	6	0	0	0	0	6
Warty dyskeratoma	4	0	0	1	0	5
Acantholytic dyskeratoma	4	0	0	0	1	5
Epidermolytic acanthoma	5	0	0	0	0	5
Melanoacanthoma	5	0	0	0	0	5

**Conclusions:** We found high IL-36 expression in PK, similar to psoriasis. Consequently, distinguishing PK and psoriasis primarily depends on clinical presentation, necessitating rigorous clinicopathologic correlation. Furthermore, the relatively frequent IL-36 expression in seborrheic keratosis may suggest a link between PK and seborrheic keratosis, with PK potentially representing a variant of inflamed seborrheic keratosis. Unlike previous observation of high IL-36 expression in lichen planus, lichen planus-like keratosis exhibits only focal and weak IL-36.

#### 431 Primary Female Urethral Mucosal Melanoma: Retrospective Analysis of Clinicopathological and Molecular Features

Volha Lenskaya<sup>1</sup>, Yunyi Wang, Anais Malpica<sup>1</sup>, Curtis Pettaway<sup>1</sup>, Jing Ning<sup>1</sup>, Jonathan Curry<sup>1</sup>, Carlos Torres-Cabala<sup>1</sup>, Phyv Aung<sup>1</sup>, Woo Cheal Cho<sup>1</sup>, Doina Ivan<sup>1</sup>, Victor Prieto<sup>1</sup>, Jeffrey Gershenwald<sup>1</sup>, Michael Davies<sup>1</sup>, Andrew Futreal<sup>1</sup>, Jennifer McQuade<sup>1</sup>, Priya Nagarajan<sup>1</sup>

<sup>1</sup>The University of Texas MD Anderson Cancer Center, Houston, TX

**Disclosures:** Volha Lenskaya: None; Yunyi Wang: None; Anais Malpica: None; Curtis Pettaway: None; Jing Ning: None; Jonathan Curry: None; Carlos Torres-Cabala: None; Phyv Aung: None; Woo Cheal Cho: None; Doina Ivan: None; Victor Prieto: None; Jeffrey Gershenwald: None; Michael Davies: None; Andrew Futreal: None; Jennifer McQuade: None; Priya Nagarajan: None

**Background:** Primary female urethral mucosal melanoma (PFUM) is exceedingly rare, accounting for <1% of all melanomas and <4% of all urethral tumors. Since they are often evaluated together with other female genital tract melanomas, the clinicopathological and molecular features that are unique to PFUM are unknown.

**Design:** In this retrospective study, we identified 20 PFUM and recorded clinicopathological and molecular features. Univariate Cox regression model was used to assess associations between recorded characteristics.

**Results:** Most patients (pts) were White (n=18, 90%) with median age of 70 years (range: 43-92); bleeding was the most common presenting symptom (n=11, 55%). PFUM were most commonly lobulated, amelanotic masses (n=14, 70%), located in the distal urethra (n=16, 80%) with involvement of urethral meatus, vagina and bladder in 50%, 40% and 30%, respectively. Relevant histopathologic features included lentiginous growth pattern (n=14, 70%); submucosal invasion (n=15, 75%); tumor thickness >4mm (n=15, 75%; median: 8.6mm, range: 3.4-25.0); ulceration (n=17, 85%); mitotic rate >10/1mm<sup>2</sup> (n=14, 70%); lymphovascular invasion (n=10, 50%) and perineural invasion (n=4, 20%). Next generation sequencing performed on 16 cases revealed mutations involving TP53 (n=3), KIT (n=3), NF1 (n=3), TERT (n=2), SF3B1 (n=2), AXL (n=1), CTNNB1 (n=1), EGFR (n=1), FGFR3 (n=1), MSH2 (n=1), PIK3CA (n=1), and NRAS (n=1), and amplification of KIT, KDR, NOTCH1, PDGFRA, CDK4, and MDM2 genes. At presentation, 14 (70%) pts had localized disease, 2 (10%) had regional and 4 (20%) had distant metastases. With 68 months of median follow-up, 9 (45%) and 15 (75%) pts developed regional and distant metastases, respectively. Median time to regional and distant metastasis were 3.6 (range: 0.6-19.8) and 6.2 (range: 1.8-57.3) months from the date of diagnosis, respectively. Thirteen pts died and 11 (55%) died due to progression of PFUM. Increasing tumor thickness correlated with locally advanced disease (p=0.035) and distant metastasis at presentation correlated with shorter disease specific survival (p=0.045).

**Conclusions:** In this exploratory analysis, we found that PFUM is an aggressive malignancy predominantly affecting older White women, with high risk for metastasis and disease-specific mortality; the genetic alterations are distinct from cutaneous melanoma as well. Certain clinicopathological features associated with worse prognosis. Studies using larger cohorts are essential for better risk stratification and treatment.

### 432 Genomic and Transcriptomic Characterization of Protein Kinase C Fusion Melanocytic Neoplasms with Distinctive Hypopigmented Histomorphology: A Single-Institution Study of 5 Cases

Aofei Li<sup>1</sup>, Brandon Umphress<sup>2</sup>, Carina Dehner<sup>1</sup>, Carli Whittington<sup>1</sup>, Simon Warren<sup>1</sup>, Ahmed Alomari<sup>1</sup>

<sup>1</sup>Indiana University School of Medicine, Indianapolis, IN, <sup>2</sup>Indiana University, Indianapolis, IN

**Disclosures:** Aofei Li: None; Brandon Umphress: None; Carina Dehner: None; Carli Whittington: None; Simon Warren: None; Ahmed Alomari: None

**Background:** Genomic fusions involving Protein Kinase C (PRKC) have been classically associated with heavy melanin pigmentation in a subset of melanocytic neoplasms. The understanding and classification of these tumors are evolving, with recently proposed reclassification from pigmented epithelioid melanocytoma (PEM) category to the blue nevus (BN) category in the fifth edition of the World Health Classification (WHO) of Skin Tumors.

**Design:** Herein, we report a series of 5 non-pigmented/hypopigmented PRKC fusion melanocytic tumors to further expand on the morphology of this entity and present a novel comprehensive molecular characterization. Clinical, histopathologic, and immunohistochemical findings were reviewed. Next-generation sequencing (NGS) data on genomic and transcriptomic levels were explored.

**Results:** The patients presented over a wide age range (7-54) at various anatomical locations (from scalp to ankle). Histomorphology shows dermal-based proliferations of non-pigmented medium-sized melanocytes with a biphasic pattern of hypercellular areas composed of nevic/epithelioid cells and hypocellular areas with dense fibrotic stroma and “collagen trapping”. High-risk features including significant atypia and mitotic activity are not identified. Immunohistochemistry mostly shows retained p16 and preserved BAP1. The clinical courses were uncomplicated after excisions. NGS reveals 2 cases of PTPRJ:PRKCB fusion and 3 cases of PRKCA fusions with partners SLC44A1, RNF13, and ATP2B4. Pathogenic secondary genomic alterations are rare and sporadic, including ATM stop-gain mutation and WT1 germline loss. RNA differential expression analysis against 6 GNAQ/GNA11-driven low-risk BNs shows a group of genes with significantly higher transcription levels, including LOXL4, RNF157, BCHE, and GDF15. Interestingly, gene set pathway analysis shows strong enrichment in microphthalmia-associated transcription factor (MITF) related genes, and yet, the tumors all lacked any significant pigmentation.

**Conclusions:** We further expand the morphologic spectrum of PRKC fusion melanocytic tumors with molecular characterization. Our novel transcriptome-level findings provide insight into the nuanced molecular events and new evidence for classification.

### 433 Clinicopathologic and Molecular Characterization of Conjunctival Melanoma in a Multi-institutional Study

Dinesh Pradhan<sup>1</sup>, Rebecca Manzo<sup>1</sup>, Bethany Batson<sup>2</sup>, Arivarasan Karunamurthy<sup>2</sup>, Raja Seethala<sup>3</sup>, Somak Roy<sup>4</sup>, Julie Youngs<sup>1</sup>, Scott Lauer<sup>1</sup>, Dominick DiMaio<sup>1</sup>, Joseph Khoury<sup>1</sup>

<sup>1</sup>University of Nebraska Medical Center, Omaha, NE, <sup>2</sup>University of Pittsburgh Medical Center, Pittsburgh, PA, <sup>3</sup>University of Pittsburgh School of Medicine, Pittsburgh, PA, <sup>4</sup>Cincinnati Children's Hospital Medical Center, Cincinnati, OH

**Disclosures:** Dinesh Pradhan: None; Rebecca Manzo: None; Bethany Batson: None; Arivarasan Karunamurthy: None; Raja Seethala: None; Somak Roy: None; Julie Youngs: None; Scott Lauer: None; Dominick DiMaio: None; Joseph Khoury: None

**Background:** Primary conjunctival melanoma (PCoM) is an unusual, highly aggressive malignancy with poor prognosis. The risk of metastatic disease is as high as 30%, and the 10-year disease-specific mortality is 9–35%. PCoM is inherently distinct from other mucosal, uveal and skin melanomas; however, its molecular pathogenesis is poorly understood hindering the development of targeted therapy.

## ABSTRACTS | DERMATOPATHOLOGY

**Design:** A total of 18 patients with PCoM were identified retrospectively from the archives of two institutions over a period of 30 years (11 patients from one; 7 from the other). Three conjunctival nevi (CN) were also analyzed for comparison. Demographic and clinicopathologic features were reviewed. Mutation profiling was performed using next generation sequencing (NGS) with a customized targeted 32-gene panel.

**Results:** The median age of the 18 PCoM and 3 CN pts was 70.5 years (range 39-94) and 52 years (range 31-56), respectively. The M: F ratio was 1.25:1 and 2:1 for PCoM and CN, respectively. The mean tumor thickness was 1.9 mm. All 3 CNs harbored activating NRAS codon 61 mutations (Q61R, Q61K and Q61K). PCoM harbored at least one pathogenic mutation in the 8 cases (100%) in which NGS was performed, and two cases had 3 or more mutations. Genomic alterations in BRAF (S467L & V600E) and NRAS (Q61H & Q61R) were the most frequent. Additional mutations included EIF1AX(N4Y), EGFR (M600T), PDGFRA (D576N), MET (R988C), ATM (V410M), NF1(L1187F), ERBB4 (E928V), GRIN2A (D369N), PREX2 (E414K) and STK19 (D89N). Interestingly, activating mutations in BAP1, KIT, SF3B1, GNAQ, and GNA11 were not identified in any of the studied cases. Seven patients had recurrences of the CoM, 1-10 years after initial diagnosis and excision, while 2 patients had local recurrence as well as metastasis (to lymph node in one pt and LN as well as distant in other). After a mean follow up of 78.3 months, 11 pts were alive with no evidence of disease, 1 was alive with disease (margin positive) and 6 pts had died, 2 of other cause and 4 of unknown cause.

Clinicopathologic and Molecular Characterization of Conjunctival Melanoma									
Case	Age	Gender	Thickness (mm)	PAM with atypia	Molecular Alteration	Recurrence (R) or Metastasis (M)	Follow up (months)	Status	
1	73	M	1.5	Yes	N/A	None	24	NED	
2	84	M	1	No	N/A	R	84	NED	
3	67	M	2.5	No	N/A	None	8	AWD	
4	83	F	1.25	No	N/A	None	6	NED	
5	77	F	2	Yes	N/A	R	120	DOC	
6	39	F	4	No	N/A	R	120	NED	
7	58	M	1.5	No	N/A	R	48	NED	
8	58	M	2.3	Yes	N/A	R	200	NED	
9	50	M	1.8	Yes	BRAF V600E	R and M (LN)	120	NED	
10	53	M	1	Yes	N/A	None	60	NED	
11	56	M	2	Yes	N/A	None	36	NED	
12	72	M	N/A	PAM	EGFR M600T. PDGFRA D576N	R and M (LN and distant)	108	DOU	
13	53	F	N/A	No	MET R988C	None	192	NED	
14	94	F	N/A	Yes	ATM V410M	R	46	DOU	
15	94	F	2.00	Yes	NRAS Q61H. L1187F. X N4Y	NRAS Q61R. EIF1A	R	44	DOU
16	69	F	N/A	No	NRAS Q61R	None	120	NED	
17	87	F	2.60	No	ERBB4 E928V. GRIN2A D369N. PREX2 E414K. STK19 D89N	None	12	DOU	
18	80	M	1.30	PAM	BRAF S467L	None	61	DOC	

**Conclusions:** Mutational analysis of PCoM reveals a distinct mutational profile from uveal and other mucosal melanomas and shows some similarity to skin melanomas. Similar NRAS mutations in CNs and some PCoM suggest a possibility of common precursor pathway among a subset of these lesions. Molecular profiling of PCoM may be valuable in strategizing management in metastatic PCoM with therapeutically actionable alterations such as NRAS, NF1, BRAF, PDGFRA, ERBB4 and EGFR.

#### 434 Morphologic and Genomic Features of Benign, Atypical (Intermediate), and Malignant Proliferating Trichilemmal Tumors

Samira Mortazavi<sup>1</sup>, Neda Rezaee<sup>2</sup>, Eric Vail<sup>1</sup>, Wonwoo Shon<sup>1</sup>

<sup>1</sup>Cedars-Sinai Medical Center, Los Angeles, CA, <sup>2</sup>AmeriPath/Quest Diagnostics, West Hills, CA

**Disclosures:** Samira Mortazavi: None; Neda Rezaee: None; Eric Vail: None; Wonwoo Shon: None

**Background:** Proliferating trichilemmal tumor (PTT) is a rare cutaneous adnexal tumor of external root sheath derivation. Though most are benign, rare cases exhibit malignant histopathologic characteristics and aggressive clinical behavior. Significant variability in diagnostic terminology and criteria persists within the different categories of PTT, necessitating further classification improvements. We therefore undertook a morphologic and genomic study of benign, atypical (intermediate), and malignant PTT.

**Design:** Our surgical pathology archives were searched for benign, atypical, and malignant PTT. Two authors independently reviewed all available slides. Cases previously diagnosed as "atypical" or "malignant" PTT were included only if clear areas of morphologically "typical" PTT were present. We identified and assessed the morphologic features from the current WHO classification and previously published characteristics. Selected cases underwent molecular analysis by a next-generation sequencing platform and/or array comparative genomic hybridization.

**Results:** Clinical, morphologic, and genomic features of PTT are summarized in Table 1. All benign PTT demonstrated solid-cystic tumors composed of cells with trichilemmal differentiation, without significant cytoarchitectural atypia. In contrast, atypical and malignant PTT showed areas of moderate to severe cytologic atypia, with many resembling squamous cell carcinoma. Pairwise comparisons revealed that malignant PTT differed from atypical PTT by displaying an infiltrative growth pattern, peripheral stromal desmoplasia, atypical small nests or cords, and atypical mitotic figure. None of our PTT cases revealed perineural or vascular invasion. Copy number variations (CNVs) were found in all evaluated cases, frequently involving chromosomes 6, 15, and 19. Extensive and more complex CNVs were a feature of atypical and malignant PTT. TP53 mutation was also seen in 2 cases (1 benign and 1 malignant).

Table 1. Clinical, morphologic, and genomic features of benign, atypical, and malignant PTT

	Benign (N=6)	Atypical (N=11)	Malignant (N=6)
Age (median, range)	65, 33-69	64, 35-84	64.7, 41-81
Sex M:F	3:3	5:6	3:3
Location			
Scalp	6	9	5
Head and neck (non-scalp)	0	1	1
Trunk	0	1	0
Size ≥2.5cm	0/6	4/11	4/6
Infiltrative growth pattern or irregular border	0/6	1/11	6/6
Desmoplastic stroma†			
Central	1/6	8/11	2/6
Peripheral	0/6	1/11	5/6
Connection to overlying epidermis	0/6	3/11	2/6
Ulceration	0/6	1/11	2/6
Moderate to severe cytologic atypia	0/6	11/11	6/6
Atypical small nests or cords	0/6	0/11	5/6
Atypical parakeratosis	2/6	11/11	6/6
Necrosis	0/6	8/11	5/6
Dystrophic calcification	4/6	7/11	4/6
Clear cell change	2/6	5/11	4/6
Mitotic count ≥3/mm <sup>2</sup>	0/6	6/11	5/6
Atypical mitotic figure	0/6	3/11	5/6
Molecular alterations	Case 1: 6p and 15 gain. 6q loss. Case 2: 19 loss. TP53 and NOTCH1 mutations	Case 1: 17q gain and 19p loss. Case 2: 37 small deletions and gains. Case 3: 1p, 1q, 5q, 6q, 8, 11q, 12q, 12p, 17q, 18, and 20 gain. 1p, 3p, 8p, 9p, 10q, 11q, 12q, 12p, 17p, and 19 loss. Case 4: 1p, 4, 8, 9p, 10, 12p, 15, 16, 17q, and 18 gain. 1p, 2p, 3p, 17p, 19, and X loss. Case 5: 3q gain. 3p, 6p, 6q, and 19 loss.	Case 1: 6p, 14, 15, 22, and X gain. 6q loss. Case 2: 1p, 6p, and 15 gain. 3p, and 6q loss. TP53 mutation. Case 3: 2q and 8 gain. 2p, 6p, 6q, and 12q loss. Case 4: 1p, 1q, 9p, 15, and 17q gain. 1p, 3p, 4q, 6p, 6q, 8p, 9p, 11p, 12q, 13q, 17p, and 19 loss.

†Two malignant PPT demonstrated both central and peripheral desmoplastic stroma.

**Conclusions:** Our results confirm a broader morphologic and genomic spectrum of PTT. Additional more complex CNVs present in atypical and malignant PTT probably explain its higher grade cytomorphology and possibly more aggressive clinical behavior. Moreover, atypical PTT can show genomic features similar to malignant PTT, suggesting that at least some atypical PTT are likely to be "encapsulated" malignant PTT. Ongoing clinical follow-up analysis should provide further insights into the natural biology of this PTT subgroup.

### 435 Smooth Muscle Neoplasms of the Dermis and Subcutaneous Tissues

Michael Mortellaro<sup>1</sup>, Sandra Gjorgova Gjeorgjievski<sup>2</sup>

<sup>1</sup>Emory University Hospital, Atlanta, GA, <sup>2</sup>Emory University School of Medicine, Atlanta, GA

**Disclosures:** Michael Mortellaro: None; Sandra Gjorgova Gjeorgjievski: None

**Background:** An atypical intradermal smooth muscle neoplasm (AISMN) is a primary dermal smooth muscle neoplasm with nuclear enlargement, increased mitoses, and an indolent prognosis. Leiomyosarcoma is a mitotically active, malignant smooth muscle neoplasm with local recurrence and metastatic potential.

**Design:** Cases from August 2013 to August 2023 were reviewed for dermal smooth muscle neoplasms, excluding benign smooth muscle neoplasms (pilar leiomyoma), metastatic lesions and irradiated cases. Nineteen cases were further categorized by location into dermal only, dermal with minimal subcutaneous involvement, dermal and subcutaneous involvement, and subcutaneous only.

**Results:** Three cases with pure dermal location and four dermal cases with minimal subcutaneous involvement occurred in seven male patients (age range: 24-83, median: 54). All had mild to moderate cytologic atypia, mitotic activity range: 1-8 per 10 high power fields (HPF), and an infiltrative growth pattern. These cases lacked tumor necrosis, surface ulceration, local recurrence or metastatic disease after 1.5 - 55 months (median: 26 months). The seven cases from six patients (4 females and 2 males, age range: 41-86, median: 72) with dermal and significant subcutaneous involvement (>50% of tumor volume) had moderate to severe cytologic atypia, skin ulceration (three cases), focal tumor necrosis (one case) and a significant increase in mitotes (range: 4-27/10 HPF). Follow up of 2 – 69 months (median: 15.5) found one patient with local recurrence at 8 months. Five subcutaneous only cases (3 females and 2 males, age range: 60-71, median: 62) were well circumscribed, showed moderate to severe cytologic atypia, increased mitoses (range: 2-13/10 HPF) and tumor necrosis (in four of 5 cases). Follow up of 1-63 months (median: 52) identified one case with metastatic pulmonary disease after 6 months.

Figure 1 - 435

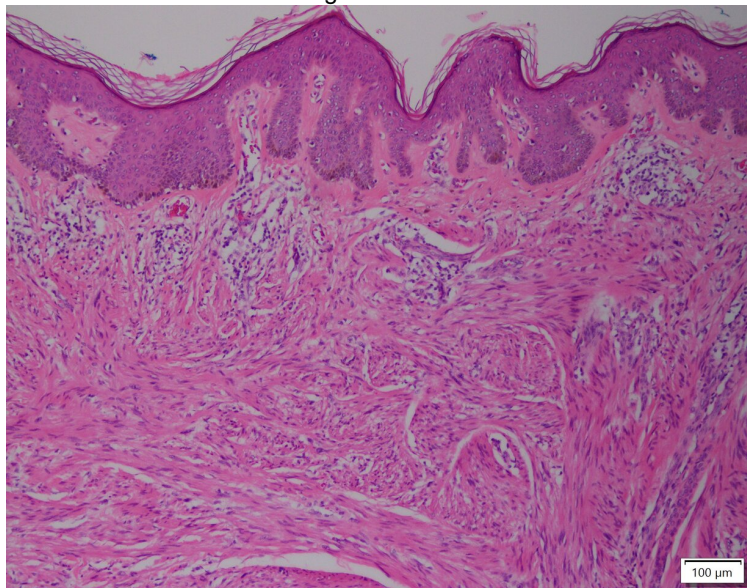
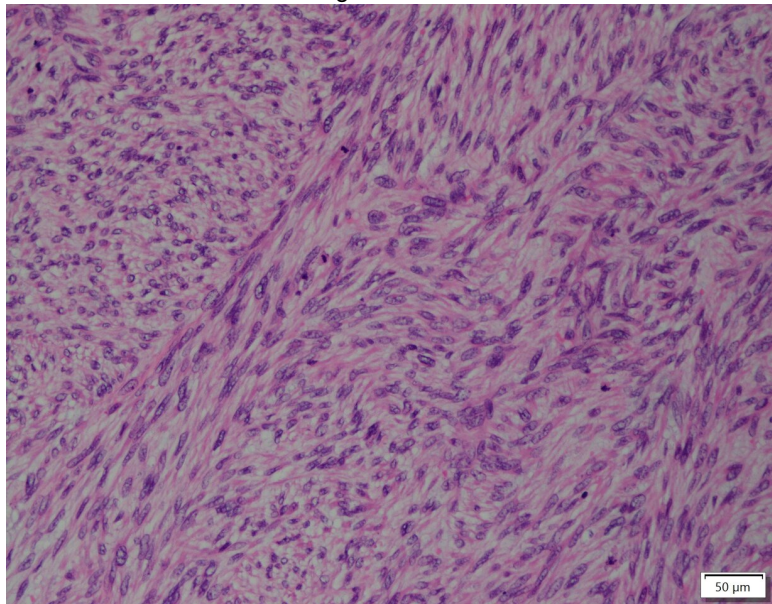


Figure 2 - 435



**Conclusions:** In our series, dermal smooth muscle neoplasms with infiltrative growth, cytologic atypia and increased mitotic activity, including those with minimal subcutaneous involvement, are seen only in males, and lack evidence of local recurrence or metastatic potential compared to smooth muscle neoplasms with significant subcutaneous involvement or that are located entirely in the subcutis. Therefore, AISMN is good terminology for these dermal lesions. "Cutaneous leiomyosarcoma" should be used for subcutaneous lesions or those with significant subcutaneous extension (>50% of the tumor volume) given their metastatic and recurrence potential.

#### 436 Molecular, Morphologic and Immunohistochemical Characterization of PRKAR1A-Mutant Melanoma

Alexander Neil<sup>1</sup>, John Hanna<sup>2</sup>, David Papke<sup>1</sup>

<sup>1</sup>Brigham and Women's Hospital, Boston, MA, <sup>2</sup>Brigham and Women's Hospital, Harvard Medical School, Boston, MA

**Disclosures:** Alexander Neil: None; John Hanna: None; David Papke: None

**Background:** *PRKAR1A* mutations are common in malignant melanotic nerve sheath tumor (MMNST), and *PRKAR1A* expression loss via immunohistochemistry (IHC) is used in diagnostic practice to distinguish MMNST from malignant melanoma. However, *PRKAR1A* alterations also have been reported in malignant melanomas that share histologic features with pigmented epithelioid melanocytoma, suggesting that *PRKAR1A* alterations have imperfect specificity in this differential diagnosis. We sought to systematically characterize *PRKAR1A* alterations in malignant melanoma along with their morphologic and IHC correlates.

**Design:** We interrogated our institutional database and identified 1,320 melanomas that underwent panel next generation sequencing. We interpreted the pathogenicity of *PRKAR1A* single nucleotide variants (SNVs), copy number variants (CNVs), and where possible, we correlated *PRKAR1A* mutation with histologic findings and *PRKAR1A* protein expression by IHC.

**Results:** *PRKAR1A* SNVs were identified in melanomas from 18 of 1,320 patients (1.4%). SNVs from 4 of 18 patients (22%) were interpreted as pathogenic, based on published characterization of pathogenicity including association with Carney complex. One pathogenic variant was missense, and the other 3 were nonsense. One of these 4 melanomas was heavily pigmented, and 3 were epithelioid; all 4 showed marked nuclear atypia that would be unusual for MMNST, and all harbored concurrent mutations typical of melanoma, including *TERT* promoter (3/4), *MAP2K1* (1/4) and *NF1* (1/4) alterations. *PRKAR1A* CNVs were identified in 176 melanomas (13.3%). 25 CNVs (13.6%) were single copy deletions, 1 was an amplification, and the others were low level gains. All 8 tested melanomas with non-pathogenic *PRKAR1A* variants (2 missense, 6 single-copy deletion) demonstrated retained *PRKAR1A* expression by IHC, while the 1 melanoma with a truncating *PRKAR1A* variant available for testing showed loss of expression. Melanomas harboring *PRKAR1A* single-copy deletions or SNVs showed pathogenic alterations in genes involved in melanoma pathogenesis (38/42 overall; 90%), including *TERT* (20/42; 48%) *BRAF* (17/42; 40%), *NF1* (11/42; 26%), and *NRAS* (9/42; 21%).

**Conclusions:** Pathogenic *PRKAR1A* mutations are rare in melanoma (4/1,320 sequenced cases; 0.3%), and most *PRKAR1A* alterations in melanoma are not pathogenic. However, because pathogenic *PRKAR1A* mutations with loss of *PRKAR1A* expression by IHC does occur in melanomas, *PRKAR1A* IHC has imperfect specificity in distinguishing MMNST from melanoma.

#### **437 Evaluating the Diagnostic Utility of MyPath® Melanoma Assay and PRAME Immunohistochemistry in Challenging Melanocytic Lesions**

Ourania Parra<sup>1</sup>, Weijie Ma<sup>2</sup>, Shaofeng Yan<sup>1</sup>, Gregory Tsongalis<sup>3</sup>, Vassiliki Kotoula<sup>4</sup>, Prodromos Hytioglou<sup>5</sup>, Konstantinos Linos<sup>6</sup>

<sup>1</sup>Dartmouth-Hitchcock Medical Center, Lebanon, NH, <sup>2</sup>Dartmouth-Hitchcock Medical Center, Geisel School of Medicine at Dartmouth, Lebanon, NH, <sup>3</sup>Dartmouth Geisel School of Medicine, Lebanon, NH, <sup>4</sup>Aristotle University of Thessaloniki, Thessaloniki, Greece, <sup>5</sup>Aristotle University Medical School, Thessaloniki, Greece, <sup>6</sup>Memorial Sloan Kettering Cancer Center, New York, NY

**Disclosures:** Ourania Parra: None; Weijie Ma: None; Shaofeng Yan: None; Gregory Tsongalis: None; Vassiliki Kotoula: None; Prodromos Hytioglou: None; Konstantinos Linos: None

**Background:** Distinguishing benign from malignant melanocytic lesions can be challenging. MyPath® Melanoma, previously known as Myriad MyPath, is a qRT-PCR assay designed to evaluate the expression of 23 targeted genes, including primarily *PRAME* and several *S100* genes. This assay serves as an adjunctive tool in differentiating benign from malignant melanocytic lesions. *PRAME* is a highly sensitive and specific marker for melanoma diagnosis. Our study sought to correlate MyPath results with *PRAME* expression, SNP array, and FISH analyses and evaluate their diagnostic utility in melanocytic lesions.

**Design:** We assessed 56 diagnostically ambiguous melanocytic lesions, categorized based on morphology into dysplastic nevi vs malignant melanoma (29), spitzoid (19), nevoid (7), and blue nevus (1). Two dermatopathologists independently reviewed the histopathologic findings, *PRAME* expression, MyPath, SNP array, and FISH results. Subsequently, lesions were definitively classified as benign or malignant. *PRAME* staining was quantified based on percentage of positive nuclei and intensity of staining, and a combined score (0-7) was calculated. SNP array was considered positive when  $\geq 3$  chromosomal aberrations were detected, or  $<3$ , but typical of melanoma. Aberrations encountered in indolent lesions, such as sole gain in 11p, were considered negative. FISH results were interpreted as normal or abnormal according to the cutoffs used by the reporting institutions.

**Results:** Thirty-eight lesions were classified as benign and 18 as malignant. SNP array results were available in 16 cases and FISH results were available in 30 cases. MyPath results showed a robust positive correlation with *PRAME* expression. Pearson's correlation coefficient further substantiated the strong association between MyPath and both *PRAME* combined score ( $r=0.81$ ,  $p<0.0001$ ) and percentage score ( $r=0.7599$ ,  $p<0.0002$ ). No significant correlation emerged between MyPath and SNP or FISH results. All the assessed markers—MyPath, *PRAME* combined score, SNP array, and FISH—demonstrated statistically significant difference between benign and malignant lesions. MyPath displayed the most robust correlation with malignancy ( $\chi^2=25.58$ ,  $p<0.001$ ), followed by *PRAME* combined score ( $\chi^2=21.37$ ,  $p<0.001$ ).

**Conclusions:** *PRAME* immunohistochemistry strongly correlates with a *PRAME*-based molecular assay and can serve as a cost-effective and rapid ancillary tool in the routine evaluation of melanocytic lesions to enhance diagnostic accuracy.

#### **438 Cutaneous Clear Cell Mesenchymal Tumors: Clear cell Tumor with Melanocytic Differentiation and ACTIN::MITF Translocation, Cutaneous PEComa and Dermal Clear Cell Mesenchymal Neoplasm**

Rodrigo Tavares Macedo<sup>1</sup>, Susan Armstrong<sup>2</sup>, Ahmed Bakhshwin<sup>3</sup>, Jennifer Ko<sup>1</sup>, Josephine Dermawan<sup>1</sup>, Steven Billings<sup>1</sup>  
<sup>1</sup>Cleveland Clinic, Cleveland, OH, <sup>2</sup>Memorial Sloan Kettering Cancer Center, New York, NY, <sup>3</sup>King Abdulaziz University, Jeddah, Saudi Arabia

**Disclosures:** Rodrigo Tavares Macedo: None; Susan Armstrong: None; Ahmed Bakhshwin: None; Jennifer Ko: None; Josephine Dermawan: None; Steven Billings: None

**Background:** Cutaneous clear cell mesenchymal neoplasms have significant morphologic and variable immunophenotypic overlap and include PEComa, dermal clear cell mesenchymal neoplasm (DCCMN) and the recently described clear cell tumor with

## ABSTRACTS | DERMATOPATHOLOGY

melanocytic differentiation and *ACTIN::MITF* translocation (CCMT with *ACTIN::MITF*), many of which are likely to have been diagnosed as PEComa prior to its recognition. The study aims to investigate a series of cases previously diagnosed as cutaneous PEComa and as DCCMN to gain more insight into these tumors.

**Design:** The institution's laboratory information system was searched (2015-2023), yielding 11 cases diagnosed as cutaneous PEComas or DCCMN. For final inclusion, cases had to have paraffin blocks or unstained slides sufficient for whole exome (WES) and whole transcriptomic sequencing (WTS).

**Results:** Ten cases met selection criteria. Amongst previously diagnosed PEComas, four cases involved the lower extremities (4/7), two involved the trunk (2/7), and one the upper extremities (1/7). Five cases were originally diagnosed as PEComas (5/7) and two as malignant PEComas (2/7). Immunohistochemical stains revealed simultaneous melanocytic (HMB-45, MITF, and/or Melan-A) and smooth muscle marker (Desmin and/or SMA) expression in three cases (3/7), while isolated expression of melanocytic markers was observed in three cases (3/7). A case was negative for both, but positive for NK1/C3 and Cathepsin-K. All cases were negative for S-100 and/or SOX-10. Three had fusions involving *MITF* and actin coding regions (*ACTB/ACTG1::MITF*) and were reclassified as CCMT with *ACTIN::MITF*, while one had concurrent *TSC2* and *WRN* mutations. The remaining 2 cases, diagnosed as malignant PEComas, harbored either an isolated *TP53* mutation, or concurrent *TP53* and *KEAP1* mutations. The tumor mutation burden (TMB) was low or indeterminate in these two malignant cases. Among the three DCCMN cases, one showed a *TP53* mutation with low TMB while the other two cases did not demonstrate either any or clinically relevant mutations. No fusions were identified in DCCMN.

Case	Age	Gender	Location	Dx	Molecular Alterations	TMB (mt(mb))
1	65	Female	Right chest	Malignant PEComa	<i>TP53</i> (c.945_949delTCCCC; p.P316fs))	Indeterminate
2	64	Female	Abdomen	Malignant PEComa	<i>TP53</i> (c.736A>G; p.M246V), <i>KEAP1</i> (c.1435G>C; p.D479H)	3
3	30	Male	Left thigh	PEComa	No genes with pathogenic alterations	1
4	64	Male	Right leg	PEComa	<i>TSC2</i> (c.5034delC; p.Y1678fs), <i>WRN</i> (c.1578delC; p.L528fs)	1
5	68	Male	Right thigh	CCMT	<i>ACTB-MITF</i> exon 3:exon 2	QNS
6	20	Female	Left lateral maleolus	CCMT	<i>ACTB-MITF</i> exon 3: exon 2	QNS
7	57	Male	Right upper arm	CCMT	<i>ACTG1-MITF</i> exon 3: exon 2	QNS
8	33	Male	Left occipital scalp	DCCMN	No genes with pathogenic alterations	1
9	34	Male	Right upper arm	DCCMN	No genes with pathogenic alterations	1
10	71	Female	Right hip	DCCMN	<i>TP53</i> (c.673-14_700del42)	3

CCMT: clear cell tumor with melanocytic differentiation and *ACTIN::MITF* translocation; DCCMN: Dermal Clear Cell Mesenchymal Neoplasm

**Conclusions:** Subsets of cutaneous PEComas are CCMT with *ACTIN::MITF*. In cases without this fusion classified as PEComa, no *TFE3* gene fusions were seen, unlike PEComas of other sites. Mutations in *TP53* and *KEAP1* were seen in cutaneous malignant PEComas which lacked a high TMB or a genetic signature that would be expected in melanomas. No fusions were identified in DCCMN; one case demonstrated mutations, but TMB was low in all cases.

### 439 Cutaneous Rhabdomyosarcoma: Analysis of NRAS/BRAF Status, Tumor Mutation Burden, and UV Signature

Veronica Ulici<sup>1</sup>, Ivy John<sup>2</sup>, Josephine Dermawan<sup>1</sup>, Arivarasan Karunamurthy<sup>2</sup>, Scott Kilpatrick<sup>1</sup>, Alexandra Isaacson<sup>1</sup>, Karen Fritchie<sup>1</sup>, Jennifer Ko<sup>1</sup>, Steven Billings<sup>1</sup>

<sup>1</sup>Cleveland Clinic, Cleveland, OH, <sup>2</sup>University of Pittsburgh Medical Center, Pittsburgh, PA

**Disclosures:** Veronica Ulici: None; Ivy John: None; Josephine Dermawan: None; Arivarasan Karunamurthy: None; Scott Kilpatrick: None; Alexandra Isaacson: None; Karen Fritchie: None; Jennifer Ko: None; Steven Billings: None

**Background:** Rhabdomyosarcomatous transdifferentiation is a rare but well-documented phenomena in both carcinoma and melanoma, and, in these cases, recognition of a conventional component by either morphology or immunophenotype is essential

## ABSTRACTS | DERMATOPATHOLOGY

for correct diagnosis. However, tumors which are entirely transdifferentiated have been traditionally impossible to differentiate from primary rhabdomyosarcoma. The introduction of novel immunohistochemistry and molecular testing, which allows for the detection of NRAS/BRAF mutations, high tumor mutation burden (TMB), and UV signature, features uncommon in sarcoma, has given us additional tools to more accurately classify these malignancies as either transdifferentiated melanoma or squamous cell carcinoma. We sought to analyze a cohort of primary cutaneous rhabdomyosarcoma to determine their NRAS/BRAF status and asses for TMB and UV signature.

**Design:** Cases diagnosed as cutaneous rhabdomyosarcoma were retrieved. The tumors were evaluated for the presence or absence of melanoma in situ (MIS) and/or epithelial dysplasia. NRAS Q61R and BRAF V600E immunohistochemistry was performed, and molecular data including TMB and UV signature was collected when available.

**Results:** 10 cases of cutaneous rhabdomyosarcoma were identified (8M/2F; 30-90 years; median, 83 years) presenting in the head/neck (n=7), extremity (n=2), and trunk (n=1). All tumors involved the dermis, and 4 cases extended into the subcutis. Morphologically, cases showed a sheet-like proliferation of atypical epithelioid cells with variably prominent nucleoli with brisk mitotic activity. All lesions were at least focally positive for myogenin or MyoD1 but lacked S100, SOX10 and keratin immunoreactivity. Examination of the overlying epidermis when present (n=9), showed MIS in a single case. By immunohistochemistry, 1 tumor (of 10) was positive for NRAS Q61R; all were negative for BRAF V600E (0/10). 2 additional cases had high TMB and UV signatures. Additional molecular testing in the remaining cases is ongoing. Follow-up was available in 4 patients; 3 developed metastasis (2 regional lymph nodes, 1 lung).

**Conclusions:** Cutaneous rhabdomyosarcoma have a predilection for head/neck sites, and a subset have genetic signatures that include either NRAS mutations or high TMB/UV signatures. Additionally, nodal metastases are common in this cohort. These findings raise the possibility that some cutaneous rhabdomyosarcomas may be melanoma or carcinoma with complete rhabdomyosomatous transdifferentiation.

### 440 Web-Based Dynamic Nomograms for Predicting Survivals of Patients with Cutaneous Melanoma

Huy Vuong<sup>1</sup>, Chau Bui<sup>2</sup>, Minh-Khang Le<sup>3</sup>

<sup>1</sup>University of Iowa Hospital and Clinics, Iowa City, IA, <sup>2</sup>University of Rochester Medical Center, Rochester, NY, <sup>3</sup>University of Yamanashi, Chuo, Japan

**Disclosures:** Huy Vuong: None; Chau Bui: None; Minh-Khang Le: None

**Background:** Melanoma is the most fatal skin cancer, and patients likely develop nodal and distant metastases during follow-up. Many known mutations contribute to the tumorigenesis of melanoma, but it is not well understood how these genetic alterations together affect patient outcomes. In this study, we aimed to construct and validate a prognostic nomogram incorporating clinicopathological features and molecular characteristics of cutaneous melanomas.

**Design:** Clinicopathological and molecular data from 276 melanoma patients were extracted. Cases were randomly divided into train (n = 220) and test cohorts (n = 56). In the train set, we first performed stepwise algorithms on the saturated Cox proportional hazard model followed by the inclusion of stepwise-selected variables in a survival random forest model. Subsequently, data were validated and evaluated by the dynamic Harrell's concordance index (C-index).

**Results:** In the first part of the validation, the C-index was 0.72 (95%CI=0.64-0.80) for prognosticating the disease-free survival (DFS) of the test set. We then validated the model's performance in overall survival (OS) estimation in train and test sets in the second part. The resulting C-indexes were 0.80 (95%CI=0.76-0.85) and 0.71 (95%CI=0.60-0.81). We divided train and test sets by the median score of the model into low and high scores. The survival differences were evaluated between patients with low and high scores in both training (Figure 1A, B) and test sets (Figure 1C, D). Patients with high scores had worse DFS and OS than those with low scores. Two-year DFS of low-score and high-score patients in the entire cohort were 98% (95%CI=96-100%) and 47% (95%CI=39-57%), respectively. On the other hand, the two-year OS of patients with low scores was 97% (95%CI = 95-100%), which is significantly higher than those with high scores (72% [95%CI=65%-81%]). The impact of each variable in the prediction model was calculated (Figure 2). The dynamic nomogram is available online (<https://lkhankv1995.shinyapps.io/MISP/>).

Figure 1 - 440

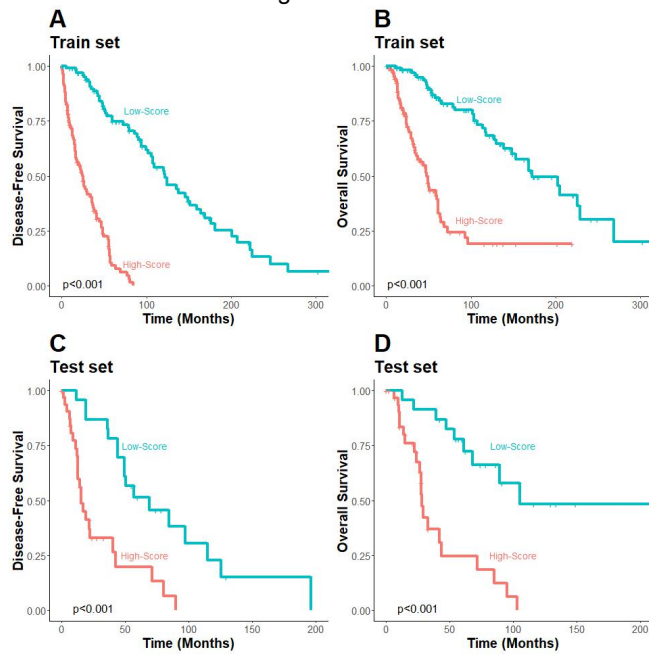
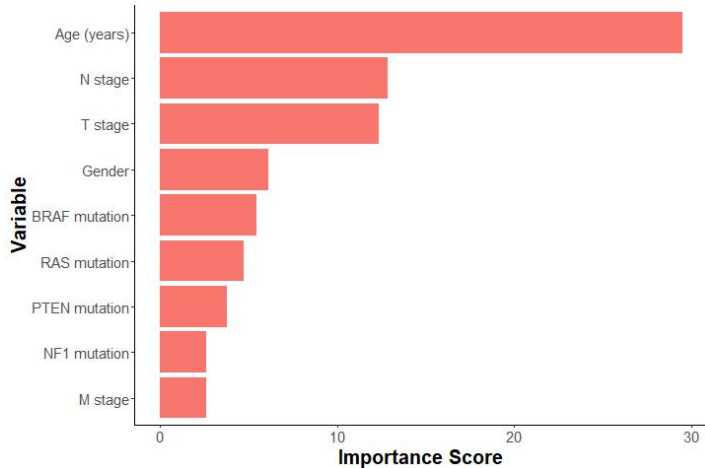


Figure 2 - 440



**Conclusions:** We developed a dynamic nomogram incorporating both clinicopathological and molecular parameters that can help precisely estimate the survival outcomes of melanoma patients. It can help clinicians better assess patient prognoses and tailor appropriate treatment decisions.

#### 441 Clinicopathological and Prognostic Implications of Merkel Cell Carcinoma Polyomavirus (MCPyV) in Merkel Cell Carcinoma: A Multicenter Study

Huy Vuong<sup>1</sup>, Minh-Khang Le<sup>2</sup>, Chau Bui<sup>3</sup>, Tetsuo Kondo<sup>2</sup>, Andrew Bellizzi<sup>1</sup>

<sup>1</sup>University of Iowa Hospital and Clinics, Iowa City, IA, <sup>2</sup>University of Yamanashi, Chuo, Japan, <sup>3</sup>University of Rochester Medical Center, Rochester, NY

**Disclosures:** Huy Vuong: None; Minh-Khang Le: None; Chau Bui: None; Tetsuo Kondo: None; Andrew Bellizzi: None

**Background:** It has been well established that polyomavirus (MCPyV) can drive the tumorigenesis of Merkel cell carcinoma (MCC). In this multicenter study, we aimed to investigate the clinical and prognostic implications of MCPyV in MCC patients.

## ABSTRACTS | DERMATOPATHOLOGY

**Design:** We retrospectively collected 124 MCC cases from the archives of three institutions. MCPyV status was assessed using the CM2B4 immunohistochemistry in 73 cases. Chi-square, Fisher's exact test, and Wilcoxon's test were used to compare categorical and continuous variables, when applicable. For time-to-event outcomes such as metastasis-free survival (MFS), recurrence-free survival (RFS), and overall survival (OS), Kaplan-Meier and multivariate Cox proportional hazard regression analyses were utilized by calculating hazard ratios (HRs) and their 95% confidence interval (CI).

**Results:** The clinicopathological characteristics of MCPyV-positive and MCPyV-negative cases are shown in Table 1. The incidence of MCPyV in MCCs was 43% and not significantly different between institutions ( $p=0.697$ ). There were no statistical differences in patient age, gender, T stage, M stage, radiation, or chemotherapy administration between the two groups. On the other side, lymph node metastasis was more frequent in MCPyV-positive MCCs ( $p=0.045$ ). Regarding tumor location, MCPyV-positive MCC was more frequently identified in the acral sites but less commonly seen in the head and neck region ( $p=0.002$ ) compared to MCPyV-negative cases. Kaplan Meier analyses demonstrated a trend toward worse prognoses in MCPyV-negative tumors, but statistical significance was not reached (Figure 1). In multivariate Cox proportional hazard regression analyses, we found a statistically significant association of improved MFS ( $HR=0.21$ ; 95% CI=0.08-0.56;  $p=0.002$ ) and OS ( $HR=0.18$ ; 95% CI=0.07-0.47;  $p<0.001$ ) in MCPyV-positive versus MCPyV-negative MCCs (Figure 2).

Variables	Polyoma-negative MCCs (n=43)	Polyoma-positive MCCs (n=30)	p-value
<b>Mean age (range)</b>	78 (31-94)	71 (47-94)	0.15
<b>Gender</b>			0.77
Women	8 (18.6%)	7 (23.3%)	
Men	35 (81.4%)	23 (76.7%)	
<b>T stage</b>			0.073
T1	15 (42.9%)	8 (30.8%)	
T2	8 (22.9%)	5 (19.2%)	
T3	1 (2.9%)	7 (26.9%)	
T4	1 (2.9%)	0 (0.0%)	
TX	10 (28.6%)	6 (23.1%)	
<b>N stage</b>			0.043
N0	19 (54.3%)	9 (34.6%)	
N1	13 (37.1%)	17 (65.4%)	
NX	3 (8.6%)	0 (0.0%)	
<b>M stage</b>			1
M0	19 (54.3%)	15 (57.7%)	
M1	9 (25.7%)	6 (23.1%)	
MX	7 (20.0%)	5 (19.2%)	
<b>Primary Location</b>			0.002
Head and Neck	24 (55.8%)	6 (20.0%)	
Trunk	8 (18.6%)	3 (10.0%)	
Upper Extremity	6 (14.0%)	11 (36.7%)	
Lower Extremity	3 (7.0%)	8 (26.7%)	
Unknown	2 (4.7%)	2 (6.7%)	
<b>Chemotherapy</b>			0.294
No	19 (44.2%)	9 (30.0%)	
Yes	8 (18.6%)	10 (33.3%)	
Unknown	16 (37.2%)	11 (36.7%)	
<b>Radiation</b>			0.644
No	10 (23.3%)	5 (16.7%)	
Yes	16 (37.2%)	14 (46.7%)	
Unknown	17 (39.5%)	11 (36.7%)	

Figure 1 - 441

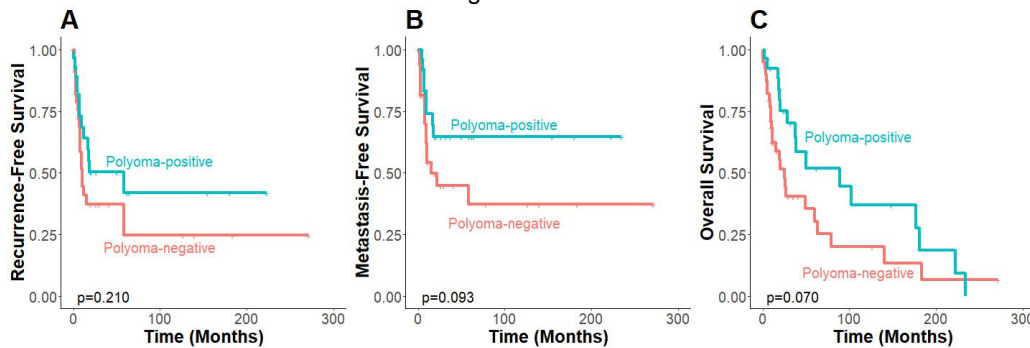
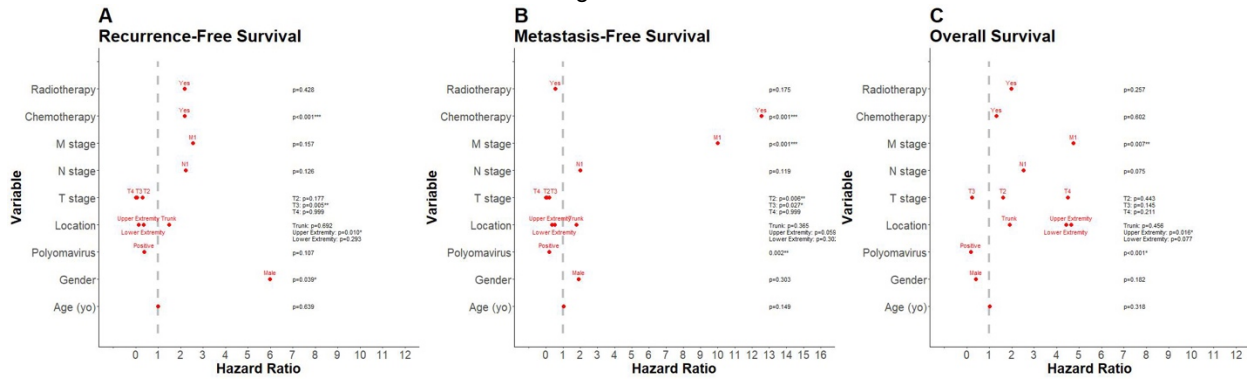


Figure 2 - 441



**Conclusions:** This study confirmed that polyomavirus is commonly seen in MCCs. MCPyV-positive and MCPyV-negative MCCs had distinct clinicopathological features. In comparison to MCPyV-driven tumors, MCPyV-negative MCCs were associated with worse survival outcomes.

## 442 Cutaneous Desmoid-type Fibromatosis: Clinicopathologic Analysis of a Rare Clinical Subtype

Craig Wakefield<sup>1</sup>, David Papke<sup>1</sup>, Christopher Fletcher<sup>1</sup>, Leona Doyle<sup>2</sup>

<sup>1</sup>Brigham and Women's Hospital, Boston, MA, <sup>2</sup>University College Dublin, Dublin, Ireland

**Disclosures:** Craig Wakefield: None; David Papke: None; Christopher Fletcher: None; Leona Doyle: None

**Background:** Desmoid fibromatoses are locally aggressive, deep-seated fibroblastic neoplasms characterized by mutations in *CTNNB1* and less often *APC*. Palmar and plantar fibromatoses are referred to as 'superficial fibromatoses' but arise in deep aponeurotic tissue. Primary cutaneous or true superficial desmoid-type fibromatosis is exceptionally rare and its clinical significance unknown; this study describes the clinicopathologic features and outcomes of ten such tumors.

**Design:** Cases involving only dermis and/or superficial subcutaneous tissue were identified from departmental and consultation files. Clinical, histologic and immunohistochemical features, as well as outcomes, were evaluated.

**Results:** There were 7 female and 3 male patients with a median age of 39 years (range 24-75). None had a history of familial adenomatous polyposis. Four patients had antecedent local trauma. Median tumor size was 2.7cm (range 1-10.5). Lesions involved trunk (n=6), extremities (n=3) and head & neck (n=1). Grossly, most were well circumscribed nodules. Suggested pathologic diagnoses included fibromatosis, hypertrophic scar, nodular fascitis, and low-grade sarcoma. Tumors were dermally confined (n=4), showed focal extension into subcutis (n=3) or only involved superficial subcutis (n=3). Tumors were composed of long fascicles of uniform spindled cells in a collagenous stroma. Two had a prominent myxoid stroma and 7 had a Grenz zone. There was frequent displacement and compression of native adnexal structures. Scattered, atypical hyperchromatic cells were present in one case. Mitotic activity was minimal. All tumors showed nuclear expression of beta-catenin (10/10), 87% showed expression of SMA (7/8), and CD34 was negative (0/4). Trisomy 8 and 20 was identified in one tumor. Follow up data were available for 6 cases (range 1-12y; median 5.5y). One patient (tumor size 9 cm) developed local recurrence, underwent

chemoradiation and was alive with disease at last follow up; no other patient had recurrence, including one with positive resection margins.

**Conclusions:** Desmoid-type fibromatosis is extremely rare in skin & subcutis and shows similar histologic features to deep-seated tumors; while the risk of recurrence appears much lower, there is potential for local progression. Diagnostic clues include a long fascicular growth pattern, compressed adnexa (in contrast to appendageal atrophy of scar), and in some cases a myxoid stroma. Immunohistochemistry for beta-catenin is usually essential to confirm the diagnosis.

### 443 Protein Kinase R-like Endoplasmic Reticulum Kinase (PERK) Immunoexpression and Gene Expression Profile of the Tumor Microenvironment of Acral Melanoma

Michael Zaleski<sup>1</sup>, Dinesh Pradhan<sup>2</sup>, George Jour<sup>3</sup>, Wei-Lien (Billy) Wang<sup>1</sup>, Denai Milton<sup>1</sup>, Victor Prieto<sup>1</sup>, Carlos Torres-Cabala<sup>1</sup>, Phyu Aung<sup>1</sup>

<sup>1</sup>The University of Texas MD Anderson Cancer Center, Houston, TX, <sup>2</sup>University of Nebraska Medical Center, Omaha, NE, <sup>3</sup>NYU Langone Health, New York, NY

**Disclosures:** Michael Zaleski: None; Dinesh Pradhan: None; George Jour: *Consultant* - BMS; Wei-Lien (Billy) Wang: None; Denai Milton: None; Victor Prieto: *Consultant* - Castle; Orlucent; Carlos Torres-Cabala: None; Phyu Aung: None

**Background:** Immunotherapies (IT) work by regulating the tumor microenvironment (TME) and have shown striking results as a treatment for advanced melanoma; however, meaningful responses are seen in only a subset of patients. Acral melanoma (AM) is a rare, aggressive type of melanoma with a distinct genetic profile. Our knowledge of the TME in rare subtypes is limited. Herein, we aimed to investigate the TME in primary acral lentiginous melanoma (PALM) and compare it with primary cutaneous melanoma (PCM) and primary non-lentiginous acral melanoma (PNLAM) to identify potential therapeutic and predictive biomarker.

**Design:** Differential gene expression (DGE) analysis was performed on 18 PALM, 9 PCM, and 8 PNLAM with a customized 770-gene expression panel (including 24 different immune cell types and 30 common cancer antigens). IHC staining for protein kinase R-like endoplasmic reticulum kinase (PERK) was performed on 25 ALM (19 primary, 6 metastatic), 9 PCM, and 9 PNLAM. Molecular and IHC findings were correlated with clinicopathologic parameters, therapy and disease-specific and overall survival.

**Results:** A prominent finding was PERK immunoexpression was significantly more common in ALM cases (40%) than in PCM (0%) and PNLAM cases (11%) ( $p=0.038$ )(Fig 1). However, IHC staining was not significantly associated with other clinicopathologic parameters or survival. DGE identified significant upregulation of *ICAM3*, *CD164*, *YTHDF2*, *IFNAR1*, *TNFSF13*, and *TYK2* in PALM cases ( $p<0.01$ ), which correlated with enrichment in the PI3K/Akt/mTOR, NF-kB, TNF, ERK, adhesion, and chemokine pathways ( $p<0.01$ ). PALM and PCM TMEs showed a significant predominance of cytotoxic CD8+ T cells (CD8+T) compared to PNLAM ( $p<0.001$ ;  $p<0.01$ )(Fig 2). PCM had a greater proportion of mast cells than PALM and PNLAM ( $p<0.01$ ). PNLAM TME showed significantly less CD8+T signature. Most PALM showed relative abundance of CD8+T over exhausted CD8+T and Tregs ( $p<0.01$ ), and these cases significantly associated with stage I/II presentation and epithelioid cytology ( $p<0.05$ ). PALMs with exhausted CD8 signatures significantly associated with ulceration and PNI ( $p=0.01$ )

Figure 1 - 443

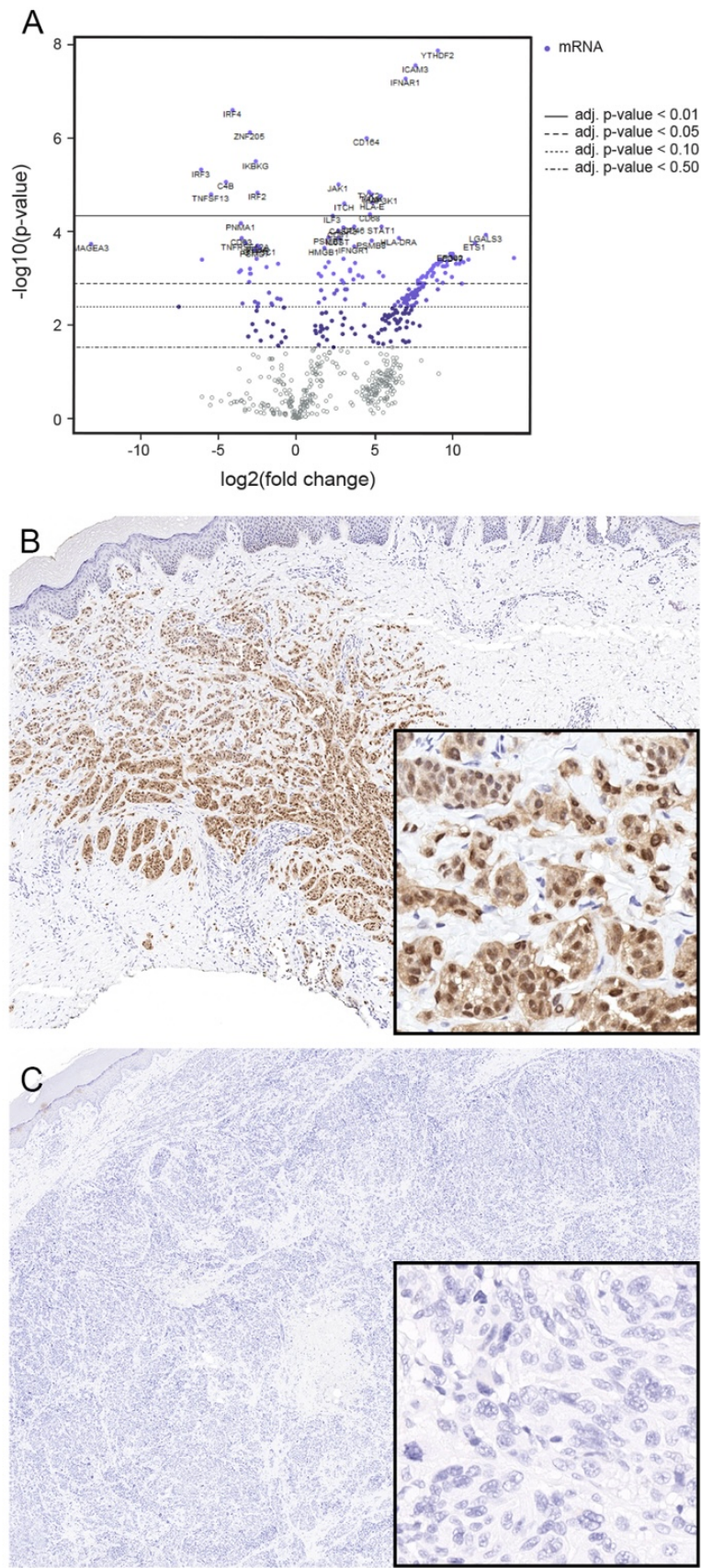
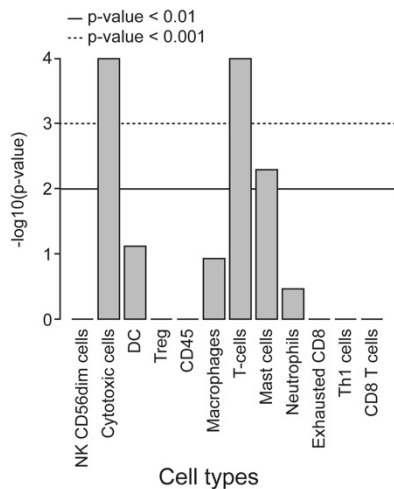
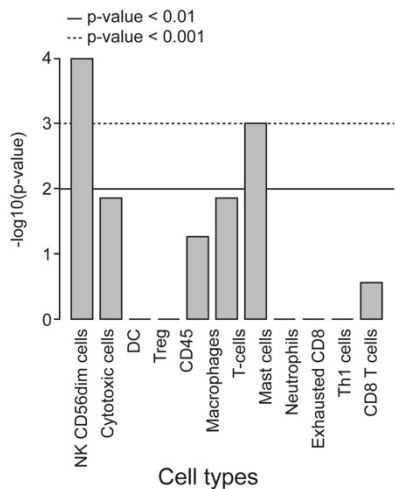


Figure 2 - 443

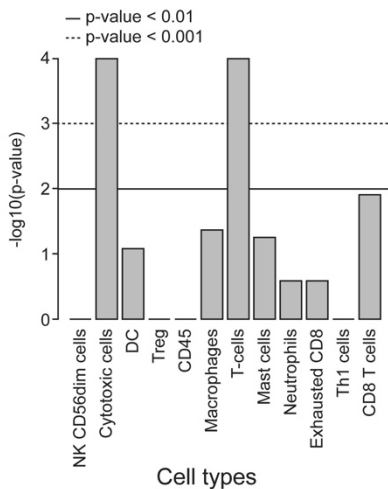
**A. PALM**



**B. PCM**



**C. NLAM**



**Conclusions:** IHC and DGE unveil that PALM is significantly different from PCM and PNLM. PALM TMEs are distinct from PNLM TME, showing a significant preponderance of CD8+ T cells over T-regs, suggesting possibly better response to IT in PALM. Upregulation of *TYK2* and *TNF* in PALM suggests the potential efficacy for combination regimen with selective TYK2 or TNF1 inhibitors when IT alone fails. Finally, upregulation of *TYK2* and *TNF* in PALM cases is supported by significantly greater immunoexpression of PERK.